Effective interaction for nucleon-nucleus scattering based on a one-boson-exchange model

K. Nakayama
Department of Physics and Astronomy, University of Georgia, Athens, Georgia 30602
and Cyclotron Laboratory, Michigan State University, East Lansing, Michigan 48824

W. G. Love
Department of Physics and Astronomy, University of Georgia, Athens, Georgia 30602
(Received 14 March 1988)

Using one of the recent Bonn potentials, an energy- and density-dependent interaction for nucleon-nucleus scattering is derived by solving the Bethe-Goldstone equation for two nucleons interacting in the presence of infinite nuclear matter at several incident energies below 425 MeV. Some of the approximations involved in the construction of the effective interaction are discussed and several of its dynamical properties are examined. Selected properties of the present interaction are also compared with those of a similar G-matrix interaction based on the Paris potential as well as with those of a recent t-matrix interaction based directly on nucleon-nucleon phase shifts. The role of medium corrections as well as the utility of the present interaction are studied by applying it to a variety of transitions in nucleon-nucleus scattering where important constraints on the transition densities are available from electron scattering.

I. INTRODUCTION

An understanding of the coupling between a projectile and the target nucleons is one of the most important elements required for studying different modes of excitation of the nucleus. One of the most significant advances[1-3] in this general area has been the inclusion of medium modifications to the nucleon-nucleon (NN) interaction at low and intermediate energies. In this work we describe the development of such a G-matrix interaction (HM86) derived from the Bethe-Goldstone (BG) equation using one of the recent one-boson-exchange (OBE) potentials derived by the Bonn collaboration.[4] Our objective here is not that of *emphasizing* differences between our interaction and the one developed by von Geramb[2] which is based on the Paris[5] potential. A valid comparison of different potentials by the G matrices they generate requires a common procedure for extracting the G-matrix interaction and implementing it, typically in a local density approximation. What we do seek is an effective interaction which is constructed in such a way that we may easily study its properties and also monitor and test the underlying assumptions used in its construction. Our overall objective is that of improving our understanding of the NN couplings relevant to calculations of nucleon-nucleus scattering.

In Sec. II we describe in some detail how the G-matrix elements are calculated in symmetric nuclear matter. We also outline how the different spin and isospin terms in the interaction are obtained from these matrix elements. The procedures for obtaining a parametrized local approximation to the G matrix are also sketched in Sec. II; this local form is especially convenient for subsequent nucleon-nucleus calculations. Also, in Sec. II, some of the underlying assumptions used in determining the G-matrix interaction are examined. In the last part of Sec. II, several of the dynamical properties of the interaction are illustrated and discussed. In Sec. III the G-matrix interaction is applied to a variety of nuclear transitions which illustrate some of its merits and deficiencies. In Sec. IV, we summarize our findings and indicate how further improvements to the NN interaction may be realized.

II. CONSTRUCTION OF THE POSITIVE ENERGY G MATRIX

A. The Bethe-Goldstone equation

The G-matrix interaction is the solution of the Bethe-Goldstone equation which, in momentum space, reads

$$G(\mathbf{K},\mathbf{k},\mathbf{k}_0)=V(\mathbf{k},\mathbf{k}_0)+\int d^3k'\frac{V(\mathbf{k},\mathbf{k}')Q(\mathbf{K},\mathbf{k}')G(\mathbf{K},\mathbf{k}',\mathbf{k}_0)}{E(\mathbf{K},\mathbf{k}_0)-E(\mathbf{K},\mathbf{k}')+i\eta}\ , \tag{2.1}$$

where $\mathbf{K}$, $\mathbf{k}$, and $\mathbf{k}_0$ denote center-of-mass (c.m.), final, and initial relative momenta, respectively. Here, the c.m. and the relative momenta are defined as

$$2\mathbf{K}_{12}=\mathbf{k}_1+\mathbf{k}_2,\quad 2\mathbf{k}_{12}=\mathbf{k}_1-\mathbf{k}_2\ . \tag{2.2}$$

In Eq. (2.1), V denotes the bare nucleon-nucleon (NN) potential; the Pauli projection operator Q restricts the two-nucleon intermediate states to those outside the Fermi distribution, F, characterized by the Fermi momentum k_F. In the energy denominator, $E(\mathbf{K},\mathbf{k})$ denotes the sum of the single-particle energies of the two interacting particles

$$E=\epsilon_1+\epsilon_2 \tag{2.3}$$

with c.m. momentum $\mathbf{K}$ and relative momentum $\mathbf{k}$; η is determined by the boundary conditions. Angle averaging of the Pauli function

$$\bar{Q}(K,k')=\frac{1}{4\pi}\int d\hat{k}'Q(\mathbf{K},\mathbf{k}') , \tag{2.4}$$

and of the energy denominator, here using Brueckner's prescription[6]

$$|\mathbf{K}\pm\mathbf{k}'|^2=K^2+k'^2\pm 2\sqrt{1/3}\bar{Q}^{3/2}(K,k')Kk' , \tag{2.5}$$

allows us to use the standard partial-wave decomposition

$$\langle SM_S' \mid G(K,\mathbf{k},\mathbf{k}_0) \mid SM_S\rangle=\frac{2}{\pi}\sum_{L'L}\sum_{J}\sum_{M_J} i^{L-L'}Y_{L'}^{M_J-M_S'}(\hat{k})Y_L^{M_J-M_S}(\hat{k}_0)^* \times(SM_S'L'M_J-M_S' \mid JM_J)(SM_SLM_J-M_S \mid JM_J)G_{L'L}^{JST}(K,k,k_0)P_T , \tag{2.6}$$

to reduce Eq. (2.1) to a set of one-dimensional coupled-channel integral equations. In Eq. (2.6) J, $L(L')$, S, and T represent the total angular momentum, the orbital angular momentum, and the total spin, and isospin, respectively. M_J and M_S (M_S') are the projections of total and spin angular momentum. P_T denotes the isospin projection operator. The resulting integral equation is

$$G_{L'L}^{JST}(K,k,k_0)=V_{L'L}^{JST}(k,k_0)+\frac{2}{\pi}\sum_{l}\int k'^2dk'\frac{V_{L'l}^{JST}(k,k')\bar{Q}(K,k')G_{lL}^{JST}(K,k',k_0)}{E(K,k_0)-E(K,k')+i\eta} . \tag{2.7}$$

Angle averaging of the Pauli function in Eq. (2.4) is a standard procedure and may be a reasonable approximation to the exact Pauli function in the case of bound state problems, where the magnitude of the c.m. momentum as defined in Eq. (2.2) is restricted to the region $0\le|\mathbf{K}|\le k_F$. The angle-averaged Pauli function $\bar{Q}$ approaches the exact function Q only when $|\mathbf{K}|$ approaches zero. In scattering problems the relevant c.m. momenta may be quite large for projectile momenta much larger than the Fermi momentum; therefore, the averaging procedure of the Pauli function may become questionable. In Sec. II B we have investigated to some extent the sensitivity of our results on $\bar{Q}$.

We use a prescription similar (but not identical) to that of Ref. 7 for the single-particle energies appearing in the energy denominator, namely:

$$\epsilon_1=\epsilon(k_1)=\begin{cases}\dfrac{\hbar^2k_1^2}{2m}+\mathrm{Re}U(k_1), & \mathrm{Re}U(k_1)<0\\ \dfrac{\hbar^2k_1^2}{2m}, & \mathrm{Re}U(k_1)\ge 0 ,\end{cases} \tag{2.8}$$

where the self-consistent potential U in symmetric ($N=Z$) nuclear matter is given by

$$U(k_1)=\sum_{2\epsilon F}\langle 12 \mid G \mid 12-21\rangle =\frac{1}{4\pi^2}\int_F d^3k_2\sum_{\substack{JST\\ L}}(2J+1)(2T+1)G_{LL}^{JST}(K,k_0,k_0) . \tag{2.9}$$

In the above equations, $k_0=|\mathbf{k}_{12}|$ and $K=|\mathbf{K}_{12}|$ as defined in Eq. (2.2).

The choice of the single-particle energy given by Eq. (2.8) is an open question. The present choice and that of Ref. 7 is motivated by the fact that, in nuclei, the particle-hole energy gap is very small (of the order of 10 MeV) compared to the corresponding gap ($\sim$60 MeV) obtained using the theoretically well established and standard "discontinuous" choice. A better and more fundamental approach, than the present one, to this problem may be the model-space method proposed in Ref. 8. In any case, when the momentum of the particle is larger than the Fermi momentum, the self-consistent potential given by Eq. (2.9) becomes a complex quantity whose imaginary part increases as the single-particle momentum increases due to the increase of the available phase space. In particular, the imaginary part becomes larger in magnitude than the real part. In spite of this we have neglected the imaginary part of the self-consistent potential in the present work; the sensitivity of our results to the choice of single-particle potential is considered in a limited way later.

The Lippmann-Schwinger integral equation for the scattering of two *free* nucleons differs from the Bethe-Goldstone equation given by Eq. (2.1) in two ways. One important difference arises from the fact that, in the Bethe-Goldstone equation, the nuclear medium produces the Pauli exclusion effect (contained in Q) which is absent from the Lippmann-Schwinger equation. Another difference appears in the energy denominator where the single-particle energy in the Lippmann-Schwinger equation includes only the kinetic energy. Since we have considered the Bethe-Goldstone equation in nuclear matter (of constant density) and have also used the angle-averaged propagator, the essential kinematical symmetries of the t and G matrices are the same (apart from the isotropic K dependence which violates Galilean invariance). Consequently, the technique for solving the G matrix may be carried over directly to the t matrix. Indeed, the t matrix (associated with V) is just the $k_F=0$ solution of the Bethe-Goldstone equation solved in the NN system. The matrix-inversion method described by Haftel and Tabakin[9] has been used to solve Eq. (2.7).

B. Extraction of the G-matrix interaction

For subsequent calculations it is especially convenient to determine the operator structure of the G matrix. This can be done by noticing that the most general two-body interaction, between identical particles of spin-$\frac{1}{2}$, which is consistent with invariance principles may be written in momentum space for each isospin state ($T=0,1$) as[10-12]

$$\begin{aligned} G=&G_0^C P_{S=0}+G_1^C P_{S=1}+iG^{LS}(\boldsymbol{\sigma}_1+\boldsymbol{\sigma}_2)\cdot\hat{\mathbf{n}} \\ &+G^T S_{12}(\hat{\mathbf{q}})+G^{T'}S_{12}(\hat{\mathbf{Q}}) \\ &+(\hat{\mathbf{q}}\cdot\hat{\mathbf{Q}})G^{T''}S_{12}(\hat{\mathbf{q}},\hat{\mathbf{Q}}),\quad \hat{\mathbf{p}}\equiv\mathbf{p}/p \end{aligned} \tag{2.10}$$

where P_S denotes the spin projection operator, $\boldsymbol{\sigma}_1$ and $\boldsymbol{\sigma}_2$ are the Pauli spin matrices, and $S_{12}(\hat{\mathbf{p}}',\hat{\mathbf{p}})$ and $S_{12}(\hat{\mathbf{p}})$ denote the tensor operators defined by

$$S_{12}(\hat{\mathbf{p}}',\hat{\mathbf{p}})\equiv\tfrac{3}{2}(\boldsymbol{\sigma}_1\cdot\hat{\mathbf{p}}'\boldsymbol{\sigma}_2\cdot\hat{\mathbf{p}}+\boldsymbol{\sigma}_1\cdot\hat{\mathbf{p}}\boldsymbol{\sigma}_2\cdot\hat{\mathbf{p}}')-\hat{\mathbf{p}}'\cdot\hat{\mathbf{p}}\boldsymbol{\sigma}_1\cdot\boldsymbol{\sigma}_2\ , \tag{2.11}$$

and

$$S_{12}(\hat{\mathbf{p}})\equiv S_{12}(\hat{\mathbf{p}},\hat{\mathbf{p}})\ .$$

In terms of the relative momenta $\mathbf{k}$ and $\mathbf{k}_0$, the three vectors $\mathbf{q}$, $\mathbf{Q}$, and $\mathbf{n}$ are defined by

$$\mathbf{q}\equiv\mathbf{k}_0-\mathbf{k},\quad \mathbf{Q}\equiv\mathbf{k}_0+\mathbf{k},\quad \mathbf{n}\equiv\mathbf{k}_0\times\mathbf{k}=\tfrac{1}{2}\mathbf{q}\times\mathbf{Q}\ , \tag{2.12}$$

so that $\mathbf{q}$ is the (direct) momentum transfer and $\mathbf{Q}$ is the exchange momentum transfer. For the coefficient of each term in Eq. (2.10) we use the notation G_s^α, where $\alpha=C$ (central), LS (spin orbit), and T (T' and T'') (tensor). These coefficients can be derived from the G matrix [Eqs. (2.1) and (2.6)] using the relations[11,12]

$$\begin{aligned} G_0^C&=\mathrm{Tr}\{GP_{S=0}\}\ , \\ G_1^C&=\tfrac{1}{3}\mathrm{Tr}\{GP_{S=1}\}\ , \\ G^{LS}&=\frac{1}{8i}\mathrm{Tr}\{G(\boldsymbol{\sigma}_1+\boldsymbol{\sigma}_2)\cdot\hat{\mathbf{n}}\}\ , \\ G^T&=\frac{1}{36\sin^4\phi}\mathrm{Tr}\{G[2S_{12}(\hat{\mathbf{q}})+(1+\cos^2\phi)S_{12}(\hat{\mathbf{Q}}) \\ &\qquad -4\cos\phi S_{12}(\hat{\mathbf{q}},\hat{\mathbf{Q}})]\}\ , \\ G^{T'}&=\frac{1}{36\sin^4\phi}\mathrm{Tr}\{G[(1+\cos^2\phi)S_{12}(\hat{\mathbf{q}})+2S_{12}(\hat{\mathbf{Q}}) \\ &\qquad -4\cos\phi S_{12}(\hat{\mathbf{q}},\hat{\mathbf{Q}})]\}\ , \\ G^{T''}&=\frac{1}{9\sin^4\phi}\mathrm{Tr}\left\{G\left[-S_{12}(\hat{\mathbf{q}})-S_{12}(\hat{\mathbf{Q}}) \right.\right. \\ &\qquad \left.\left.+\left[\frac{3\cos^2\phi+1}{2\cos\phi}\right]S_{12}(\hat{\mathbf{q}},\hat{\mathbf{Q}})\right]\right\}\ . \end{aligned} \tag{2.13}$$

Here the trace over the Pauli spin matrices $\boldsymbol{\sigma}_1$ and $\boldsymbol{\sigma}_2$ is implied and ϕ denotes the angle between $\mathbf{q}$ and $\mathbf{Q}$. The last term in Eq. (2.10) vanishes when $\hat{\mathbf{q}}\cdot\hat{\mathbf{Q}}\equiv\cos\phi=0$ as a consequence of time-reversal invariance. (This condition holds when $|\mathbf{k}_0|=|\mathbf{k}|$.) Explicit expressions for the coefficients G_s^α, in Eq. (2.13), in terms of the matrix elements $G_{L'L}^{JST}(K,k,k_0)$ are given in Refs. 11 and 12.

For some purposes it is convenient to have the G-matrix interaction in the spin and isospin *transfer* representation. Equation (2.10) may be decomposed into isoscalar and isovector components; using the explicit form of the spin and isospin projection operators one obtains

$$\begin{aligned} G=&G_0+G_\tau\boldsymbol{\tau}_1\cdot\boldsymbol{\tau}_2+G_\sigma\boldsymbol{\sigma}_1\cdot\boldsymbol{\sigma}_2+G_{\sigma\tau}\boldsymbol{\sigma}_1\cdot\boldsymbol{\sigma}_2\boldsymbol{\tau}_1\cdot\boldsymbol{\tau}_2 \\ &+iG_0^{LS}(\boldsymbol{\sigma}_1+\boldsymbol{\sigma}_2)\cdot\hat{\mathbf{n}}+iG_\tau^{LS}(\boldsymbol{\sigma}_1+\boldsymbol{\sigma}_2)\cdot\hat{\mathbf{n}}\boldsymbol{\tau}_1\cdot\boldsymbol{\tau}_2\ , \\ &+G_0^T S_{12}(\hat{\mathbf{q}})+G_\tau^T S_{12}(\hat{\mathbf{q}})\boldsymbol{\tau}_1\cdot\boldsymbol{\tau}_2\ , \\ &+G_0^{T'}S_{12}(\hat{\mathbf{Q}})+G_\tau^{T'}S_{12}(\hat{\mathbf{Q}})\boldsymbol{\tau}_1\cdot\boldsymbol{\tau}_2\ , \\ &+\hat{\mathbf{q}}\cdot\hat{\mathbf{Q}}G_0^{T''}S_{12}(\hat{\mathbf{q}},\hat{\mathbf{Q}})+\hat{\mathbf{q}}\cdot\hat{\mathbf{Q}}G_\tau^{T''}S_{12}(\hat{\mathbf{q}},\hat{\mathbf{Q}})\boldsymbol{\tau}_1\cdot\boldsymbol{\tau}_2\ . \end{aligned} \tag{2.14}$$

The relationship between the new coefficients G_β^α in Eq. (2.14), where $\beta=o,\tau,\sigma,\sigma\tau,\ldots$, and G_s^α in Eq. (2.10) may be found in Ref. 11.

Equations (2.10) and (2.14) represent the exact operator structure of the G-matrix interaction. Since the coefficients G_s^α and G_β^α are expressed in terms of the partial-wave matrix elements $G_{L'L}^{JST}(K,k,k_0)$ (see Ref. 12), this interaction depends on the initial and final relative momenta $\mathbf{k}_0$ and $\mathbf{k}$, the magnitude of the c.m. momentum $|\mathbf{K}|$ and the Fermi momentum k_F. The dependence of G on K and k_F enters through the angle-averaged Pauli projection operator $\bar{Q}$ and the single-particle energies $E(K,k)$. It should be noted that the G-matrix interaction is a complex quantity, i.e., the coefficients G_s^α and G_β^α in Eqs. (2.10) and (2.14) contain both real and imaginary parts.

Before discussing the construction of the effective G-matrix interaction, we consider two ambiguities/uncertainties encountered in constructing the G matrix; these involve the choice of the single-particle potential appearing in the energy denominator of Eq. (2.7) and the use of the angle-averaged Pauli projection operator $\bar{Q}$ of Eq. (2.4) as mentioned in the preceding section. The insensitivity of our results to the choice of single-particle potential is illustrated in Fig. 1 using the earlier Holinde-Erkelenz-Alzetta (HEA) version[13] of the Bonn potential. The modulus of the spin and isospin independent part of the on-shell ($|\mathbf{k}|=|\mathbf{k}_0|$) G-matrix interaction is shown at $k_F=1.36$ fm^{-1} as a function of momentum transfer at an incident energy of 210 MeV for two choices of the single-particle potential (U). The "full U" curve corresponds to the use of the single-particle energy

$$\epsilon(k_1)=\frac{\hbar^2k_1^2}{2m}+\mathrm{Re}U(k_1)\ ,$$

with U calculated self-consistently for single-particle momenta $k_1\le 10$ fm^{-1}. The curve denoted by "$U\le 0$" corresponds to using the same potential where $\mathrm{Re}U\le 0$ and setting it to zero for large momenta where the real part of the full self-consistent potential becomes repulsive. Even in this part of G (G_0), which is especially sensitive to short-range correlations, the differences between these two choices of U are seen to be very small.

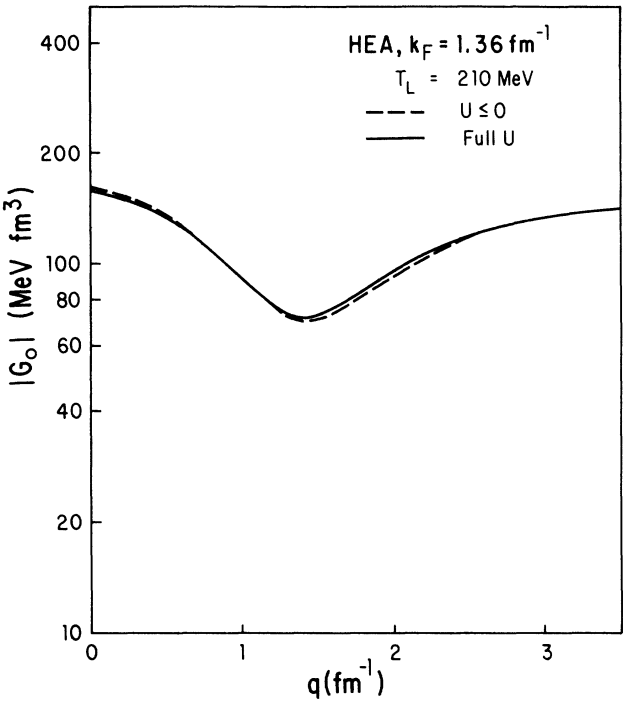

FIG. 1. Sensitivity of $|G_0|$ to choice of single-particle potential. The dashed curve corresponds to setting $U=0$ wherever it is calculated to be repulsive.

In order to discuss the uncertainty in using an angle-averaged Pauli operator, we illustrate in Fig. 2(a) the region in momentum space ($0 \le \bar{Q} \le 1$) over which the Pauli operator of Eq. (2.4) must be averaged. K denotes the c.m. momentum [see Eq. (2.2)] and k' the relative momentum in intermediate states. The values of K and k_0 were chosen to be $k=k_0=1.40$ fm^{-1}, values which significantly sample the $0 \le \bar{Q} \le 1$ region and correspond to the incident energy $T_L=140$ MeV at $k_F=1.36$ fm^{-1} according to the prescription described in Sec. II C. At $T_L=140$ MeV, angle-averaging is required along the dashed vertical line in Fig. 2(a), where $0.24 \le \bar{Q} \le 1.0$. We have explored the sensitivity of our G matrix to the use of the angle-averaged Q (i.e., $\bar{Q}$) by evaluating different components of the G matrix at zero momentum transfer for fixed values of $\bar{Q}$. The results are displayed for the HM86 interaction in Fig. 2(b) for $0.5 \le \bar{Q} \le 1.0$ at 140 MeV. A 20% change in $\bar{Q}$ corresponds roughly to a 10%, 15%, 30%, and 2% change in the modulus of G_0, G_τ, G_σ, and $G_{\sigma\tau}$ respectively; note that the modulus of G_σ is very small. The points denote the values of $|G|$ obtained in the full calculation using the momentum-dependent $\bar{Q}$. These values of $|G|$ define a $\bar{Q}$ (effective). The linearity of $|G(\bar{Q})|$ reflects the fact that both ReG and ImG depend linearly on $\bar{Q}$ and either the real or imaginary part dominates each component of G. This approximately linear behavior of $G(\bar{Q})$ may be most easily understood in terms of the integral equation relating $G(\rho)$ to $G(\rho=0)$, where ρ denotes the nuclear density. In particular,

$$G(\rho)=G(0)+G(0)\left[\frac{1}{e(0)}-\frac{Q}{e(\rho)}\right]G(\rho)\ , \tag{2.15}$$

where $e(\rho)$ is the energy denominator at density ρ as in Eq. (2.1). Unlike the Bethe-Goldstone (BG) equation [Eq. (2.1)] where V is a very poor approximation to $G(\rho)$, Eq. (2.15) has as its leading term $G(0)$ which is a reasonable first approximation to $G(\rho)$. Moreover, $G(\rho=0)$ is independent of Q so that a first iteration of Eq. (2.15) yields $G(\rho)$ which is essentially linear in the Pauli operator Q. The variation of $\bar{Q}$ (effective) with spin and isospin reflects the state dependence of the iterated terms. Figure 2(c) also illustrates the sensitivity of the isovector tensor force to $\bar{Q}$ at 140 MeV. Above $\sim$100 MeV the small Fourier components of $G_\tau^T(q)$ which arise from the long-range one-pion-exchange potential (OPEP) are seen to be insensitive to the details (strength) of the short-range correlations. At larger momentum transfers G_τ^T is sensitive to correlations in a way which has been discussed in detail in Ref. 14.

C. Construction of an energy-, density-, and momentum-transfer-dependent effective G-matrix interaction

The nuclear matter G-matrix interaction as derived in the preceding section is still too complicated to be used conveniently in nucleon-nucleus scattering calculations. It is desirable to have an effective interaction which is simple enough to be manageable in actual calculations and yet preserves the features of the "exact" G matrix which are most relevant to nucleon-nucleus scattering. It should be mentioned that there are numerous ambiguities in the procedure for determining the effective interaction from the G matrix and some of these are discussed in Refs. 1 and 15. Here we will describe briefly the particular method we have used and discuss some of the ambiguities involved.

A physical picture of the scattering problem is that in which one of the two interacting nucleons in the initial state belongs to the incident beam (above the Fermi level) and strikes the other nucleon in the target nucleus (below the Fermi level) with a given incident energy T_L. The incident energy T_L is related to the local momentum k_1 of the incident particle by

$$T_L=\frac{\hbar^2 k_1^2}{2m}+U(k_1)\ , \tag{2.16}$$

where $U(k_1)$ is the potential energy felt by the incident particle (with a local momentum k_1) due to the nucleons in the target nucleus.

In the present work we will assume that the potential energy U in Eq. (2.16) is given by the real part of the self-consistent potential defined in Eq. (2.9). With this assumption the local momentum k_1 of the incident particle can be determined from Eq. (2.16) for a given incident (and asymptotically kinetic) energy T_L. The momentum k_2 of the nucleon below the Fermi level (in the initial state) which interacts with the incident particle is, in the present work, assumed to be given by averaging over the Fermi sphere, giving

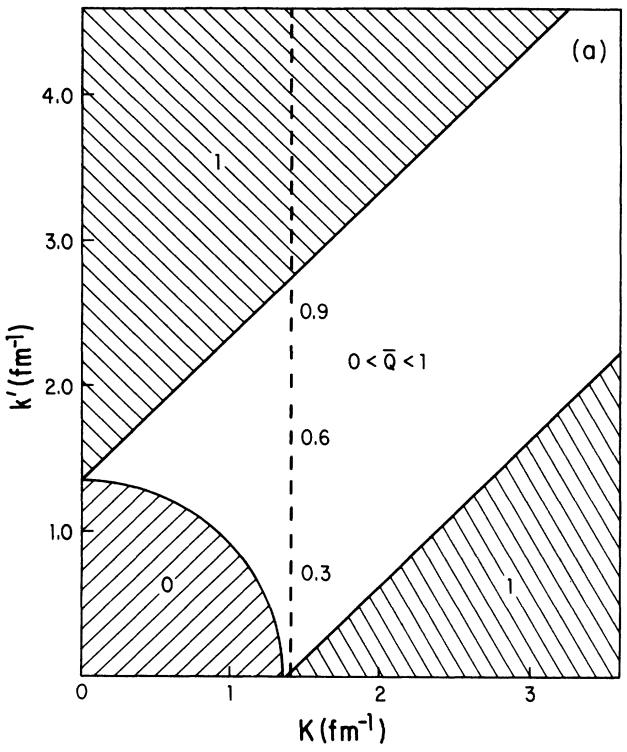

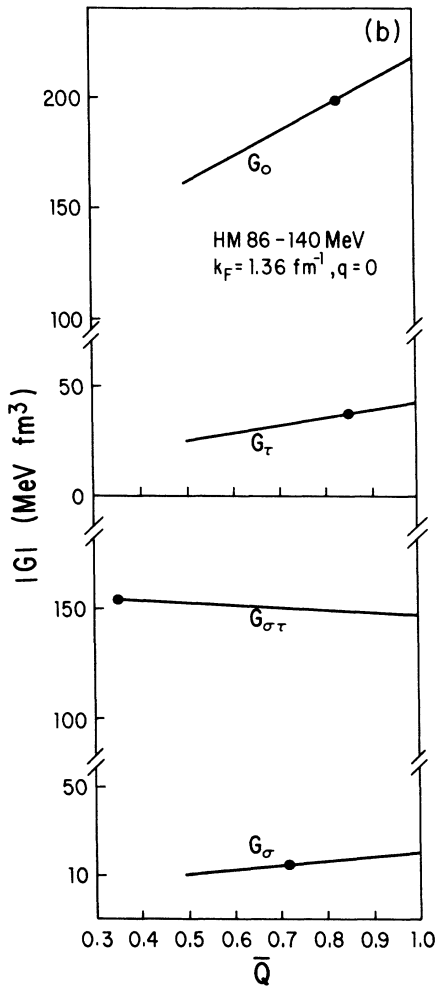

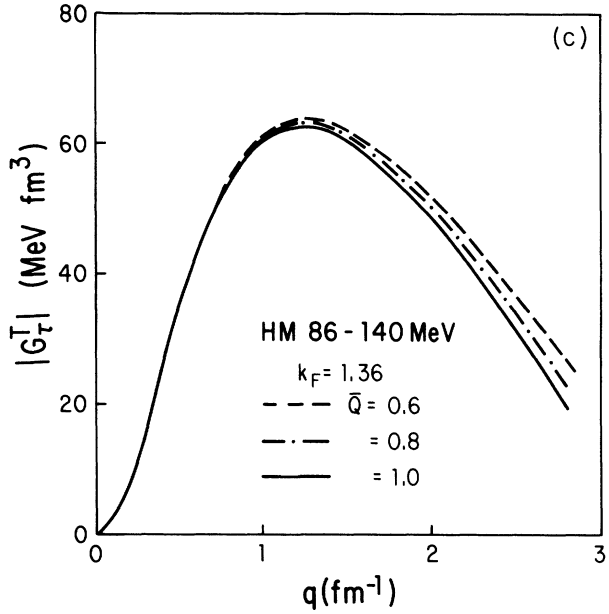

FIG. 2. (a) Domain over which the Pauli operator is and is not averaged at an incident nucleon energy of 140 MeV. The dashed vertical line corresponds to one-half the momentum of the center of mass at 140 MeV and contains the points where $\bar{Q}$ is required. The numbers to the right of this line denote the values of $\bar{Q}$ thereon. (b) Moduli of $G(k_F=1.36, q=0)$ as a function of fixed $\bar{Q}$. The points denote the values of $|G|$ obtained by using the angle-averaged $\bar{Q}$. (c) The isovector tensor force at 140 MeV for $k_F=1.36$ fm^{-1} at different fixed values of $\bar{Q}$.

$$\langle k_2 \rangle = \tfrac{3}{4} k_F \ . \tag{2.17}$$

Once the moduli and relative orientation of the momenta of the interacting particles in the initial state are fixed, the initial relative momentum $\mathbf{k}_0$ and the c.m. momentum $\mathbf{K}$ defined in Eq. (2.2) may be determined. In order to obtain a more manageable NN interaction, we have made an unweighted average over the direction of $\mathbf{k}_2$ with respect to the local momentum $\mathbf{k}_1$ of the incident particle. This yields

$$\langle k_0 \rangle = \langle K \rangle = \frac{k_>}{2} + \frac{1}{6}\frac{k_<^2}{k_>} \ , \tag{2.18}$$

where $k_>$ ($k_<$) is the larger (smaller) of k_1 and k_2. Although the averaging procedure involved here is less elaborate than those used by other authors[1,2] in the construction of the effective interaction, nonrelativistically this procedure does yield the free t matrix in the limit $k_F \to 0$; indeed, this property of the interaction was built into the method intentionally. Nonrelativistic kinematics have been used; nevertheless, we note that if the target nucleon were at rest, k_0 in Eq. (2.7) would be given correctly by $k_0 = \sqrt{m T_L/2}$ both relativistically and nonrelativistically. The error in k_1 of Eq. (2.8) is less

than 5% for $T_L \lesssim 200$ MeV where the effects of Pauli blocking are most important. This is well within the other uncertainties such as using an average value of k_2 as in Eq. (2.17).

Although Eqs. (2.10)–(2.14) give the most general structure of the G matrix in momentum space, in this work we derive the effective G-matrix interaction from its matrix elements on the energy shell, i.e., $k=k_0$ in Eq. (2.7). This procedure represents a simple (but not the most general) extension of the method used in Ref. 16 where the effective interaction was derived from the *free NN t* matrix based on a phase-shift analysis. The on-shell and near-on-shell matrix elements are expected to be the most important ones at moderate excitation energies ($E_x \ll T_L$) due to the relatively narrow spread in relative collision momenta provided by the momentum distribution of the initial and final state target wave functions. In this on-shell procedure $\hat{\mathbf{q}}\cdot\hat{\mathbf{Q}}=0$ and the $G^{T''}$ terms are absent. Equations (2.16)–(2.18) determine k, k_0, and K in terms of the incident energy T_L and the Fermi momentum k_F, so the G-matrix interaction now depends on the incident energy T_L, the Fermi momentum k_F, and the angle θ between initial and final relative momenta $\mathbf{k}_0$ and $\mathbf{k}$. θ is the scattering angle in the NN c.m. frame and is related to the momentum transfer defined in Eq. (2.12) by

$$q=2k_0\sin\frac{\theta}{2}\ ,\qquad Q=2k_0\cos\frac{\theta}{2}\ . \tag{2.19}$$

In the final stage of the construction of the effective interaction, the complex G-matrix interaction obtained from Eqs. (2.10) or (2.14) by solving Eq. (2.7) in the Pauli allowed states with the prescriptions given by Eqs. (2.16)–(2.19) was fitted at several incident energies and Fermi momenta to a sum of antisymmetrized momentum-space Yukawa (or $r^2\times$ Yukawa for the tensor force) functions as described in detail in Ref. 16. After choosing a set of ranges for the Yukawa functions at a given energy, the complex strengths were adjusted independently for each value of k_F. As in Ref. 16, the longest range part of the real *central* part of the G-matrix interaction was fixed at the value of the OPEP at all energies and densities considered. In the present work, the G matrix was calculated at the Fermi momenta k_F (fm^{-1})=0.00, 0.65, 0.95, 1.10, 1.25, and 1.36 corresponding to $\rho/\rho(k_F=1.36)$=0.00, 0.109, 0.341, 0.529, 0.776, and 1.00. The partial-wave G-matrix elements $G^{JST}_{L'L}$ were calculated for $J\le 10$, 15, and 18 for T_L (MeV) ≤ 100, $100<T_L$ (MeV) ≤ 270, and $270<T_L$ (MeV) ≤ 425, respectively. The rather large values of J included are dictated by the long range of the OPEP.

The density dependence of the effective interaction enters through the local density approximation (LDA), where the density of the target nucleus $\rho(r)$ is related to the local Fermi momentum k_F by

$$k_F(r)=\left[\frac{3\pi^2}{2}\rho(r)\right]^{1/3}. \tag{2.20}$$

D. Some limitations of the effective *G*-matrix interaction

In addition to uncertainties associated with the exact (numerical) solution of the BG equation as discussed in the preceding section, there are uncertainties associated with the approximation used here of constructing the local effective interaction as described above. The present effective interaction yields off-energy-shell ($k\neq k_0$) matrix elements which need not agree with those obtained by solving the BG equation.[17] We have estimated the extent of this off-shell disagreement by comparing the "exact" G matrix with that obtained from our multiple Yukawa representation of the effective interaction. Results for the G_0 part of the interaction are shown in Fig. 3 at $k_F=0$ and for an initial relative momentum k_0 corresponding to an incident nucleon energy of 140 MeV. For the exact G matrix, the magnitude of the final relative momentum $\mathbf{k}$ was varied while its direction was taken to be along $\mathbf{k}_0$, the initial relative momentum. This choice

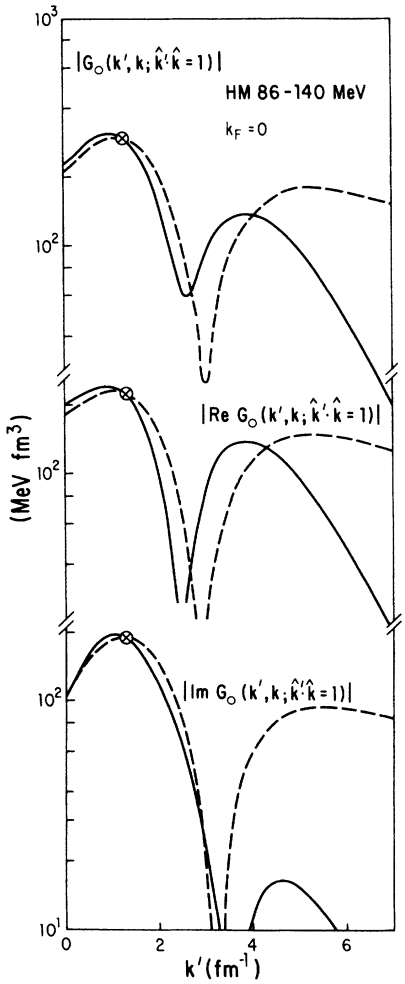

FIG. 3. Momentum dependence of G_0 at 140 MeV. The dashed curves were calculated using the local Yukawa representation of G_0 described in the text; the solid curves were obtained from the exact half-off-shell G matrix at $\hat{k}'\cdot\hat{k}=1$ as described in the text. $\mathbf{k}$ and $\mathbf{k}'$ denote the NN relative momenta before and after the collision and $\otimes$ denotes the on-shell point $k'=k$.

of kinematic conditions is in sharp contrast to the on-shell kinematics used to extract the local interaction. As shown in Fig. 3, there are sizeable differences between both real and imaginary parts of the exact and local interactions away from the on-shell point near 1.3 fm^{-1}, particularly for $k > 2.5$ fm^{-1}. Note, however, that contributions to nucleon-nucleus scattering from such significantly different relative momenta will be suppressed by the limited spread in momenta allowed by the nuclear wave functions. As a result, the misrepresentation of the off-shell elements, by the present local ansatz, while non-negligible, is likely much less important than might be supposed. Off-shell differences in the other central parts of the force exhibit a qualitatively similar behavior to that shown in Fig. 3. We are in the process of making a more precise estimate of these off-shell effects; the results will be reported elsewhere.

The multiple Yukawa representation of the effective interaction only represents nonlocality via inclusion of the Pauli principle. Various sources of nonlocality have been shown[18] to be important for understanding selected spin observables in nucleon-nucleus scattering. Here we consider briefly some of the nonlocal effects. In order to disentangle nonlocal ($r \neq r'$) from off-shell ($k_0 \neq k$) effects, we only consider the G matrix on the energy shell. In momentum space, a purely local interaction depends only on the momentum transfer $\mathbf{q}=\mathbf{k}_0-\mathbf{k}$. Therefore, one way of gauging the overall nonlocality of an interaction (including exchange terms) is to examine its dependence on $\mathbf{Q}=\mathbf{k}_0+\mathbf{k}$ at a fixed value of $\mathbf{q}$. For a local bare potential (V) nonlocality will arise from the correlated (second) term ($\tilde{G} \equiv G - V$) in Eq. (2.1) even in the absence of the Pauli principle. In the case of the OBE model, the bare potential itself is nonlocal (even without the Pauli exchange terms) so that both correlated and uncorrelated terms generally contribute to the total nonlocality of G. For example, the σ-, ω-, π-, and ρ-meson exchange contributions yield the bare potential in the NN c.m. frame:[12]

$$V(\mathbf{q},\mathbf{Q}) = -4\pi g_\sigma^2 \frac{1}{q^2+m_\sigma^2}\left[1+\frac{q^2-Q^2}{8m^2}+\frac{i}{4m^2}(\sigma_1+\sigma_2)\cdot\mathbf{n}\right] + 4\pi g_\omega^2 \frac{1}{q^2+m_\omega^2}\left[1-\frac{q^2-3Q^2}{8m^2}-\frac{3i}{4m^2}(\sigma_1+\sigma_2)\cdot\mathbf{n}\right]$$
$$-\tfrac{4}{3}\pi g_\pi^2 \frac{1}{4m^2}\frac{q^2}{q^2+m_\pi^2}[\sigma_1\cdot\sigma_2+S_{12}(\hat{q})]\tau_1\cdot\tau_2 - \tfrac{4}{3}\pi g_\rho^2\left[1+\frac{f_\rho}{g_\rho}\right]^2 \frac{1}{4m^2}\frac{q^2}{q^2+m_\rho^2}[2\sigma_1\cdot\sigma_2-S_{12}(\hat{q})]\tau_1\cdot\tau_2 , \quad (2.21)$$

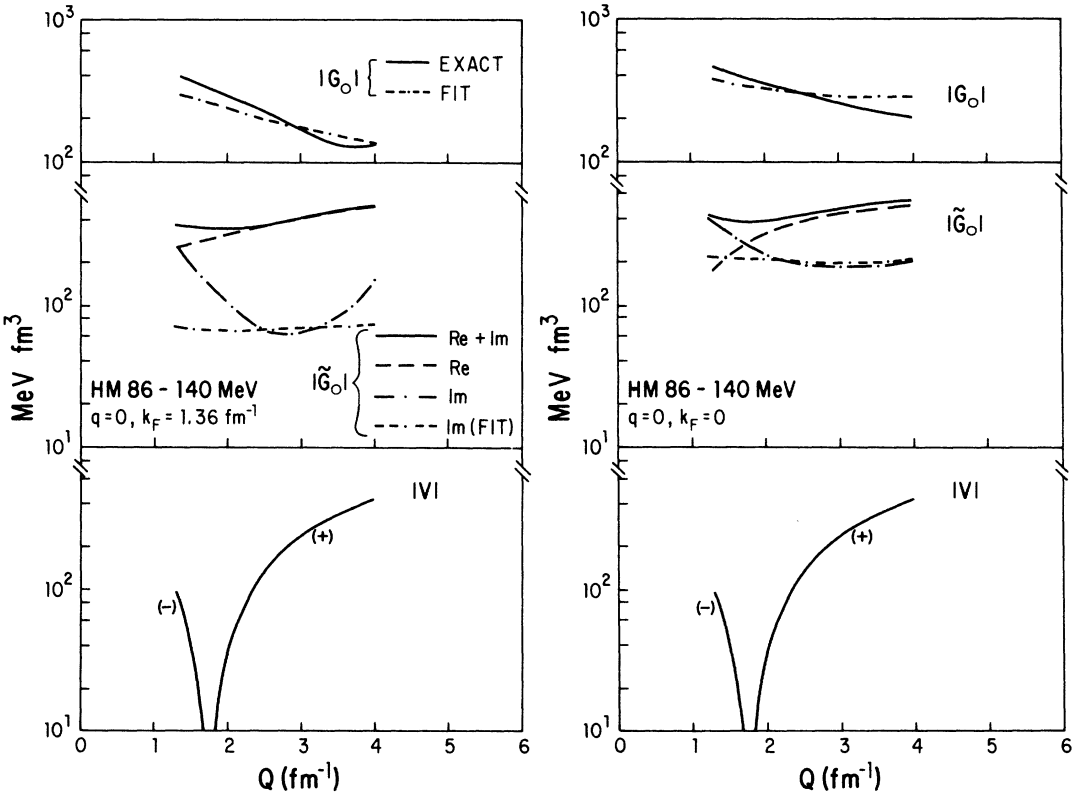

FIG. 4. Upper: nonlocality (Q dependence) of the exact and fitted versions of $|G_0|$ at 140 MeV with $k_F=0$ and 1.36 fm^{-1} and $q=0$. Middle: Q dependence of the correlated parts of G_0 (i.e., $\tilde{G}_0$) at $k_F=0$ and 1.36 fm^{-1}. Lower: Q dependence of the bare potential V at $k_F=0$ and 1.36 fm^{-1}. The − and + signs denote the attractive and repulsive regions of V, respectively.

where form factors have been omitted for simplicity and terms through order k^2/m^2 have been kept; **n** is defined in Eq. (2.12). Although the terms from π and ρ exchange are local, the terms associated with σ and ω exchange give rise to (in addition to the spin-orbit terms) significant nonlocal contributions to V at the *potential* level.

We have explored, in a limited way, the degree of nonlocality of G_0. The imaginary part of the approximate (Yukawa) representation of the correlated contribution is shown in Fig. 4 because it arises entirely from correlations when a real bare potential is used as is done here. In each case, the usual direct momentum transfer and scattering angle were set to zero. The resulting exchange momentum transfer $Q=2k_0$ was varied by varying k_2, the momentum of the struck nucleon between -1.36 and $+1.36$ fm^{-1} along the direction of k_1 at a value of k_1 corresponding to the local kinetic energy which is shifted from 140 MeV at $k_F\neq 0$ by the single-particle potential. The range of variation of k_2 was chosen to represent the Fermi motion of the target nucleons.

Figure 4 demonstrates that, based on the Q dependence, the nonlocality of the bare interaction is much larger than that of the correlated contribution. At each value of k_F we see that the nonlocality of the modulus of G_0 is described better by the multiple Yukawas than is the modulus of its imaginary part. Although the differences between the approximate (FIT) and exact values of both $\tilde{G}_0$ and G_0 appear to be non-negligible, these differences are very small near $k_2=0$ ($Q\sim 2.8$ fm^{-1}). Moreover, the variation shown in Fig. 4 is extreme in that we have assumed collinear collisions.

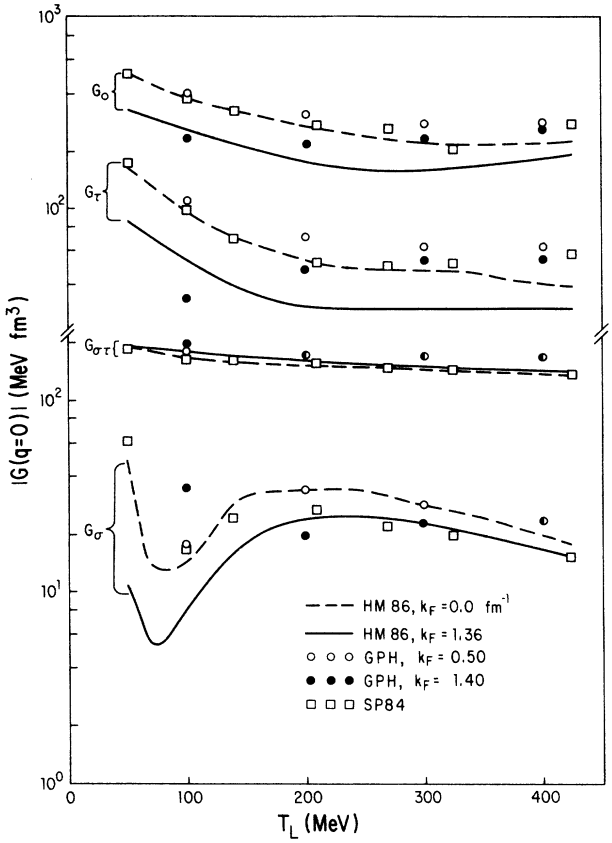

FIG. 5. Energy and density dependence of the central components of the HM86 and GPH interactions; results for the SP84 interaction are also shown.

E. Properties of the effective *G*-matrix interaction

In this section we consider some of the dynamical characteristics of the Yukawa representation of the present G-matrix interaction (HM86) based on the Bonn potential,[3] which are useful in the interpretation of nucleon-nucleus scattering. Some of these properties are compared with the free t-matrix interaction (SP84) of Refs. 16 and 19 and/or the G-matrix interaction (GPH) derived by von Geramb[2] which is based on the Paris potential.[5] These interactions include both direct and exchange terms. In this section, the exchange terms have been evaluated in an "asymptotic" energy approximation as described in Ref. 16; in particular, Q in Eq. (2.2) is fixed at $2k_0$. It should be noted that with Q fixed at $2k_0$ the exact G matrix and its Yukawa representation shall only (necessarily) agree at $q=0$ where the on-shell kinematics are realized; see Eq. (2.19).

Figure 5 illustrates the energy and density dependence of the magnitude of the central components of the HM86 (Bonn), GPH (Paris), and SP84 (phase-shift analysis) interaction at zero-momentum transfer ($q=0$). The HM86 and GPH interactions are shown at the smallest and largest Fermi momenta at which they are calculated. As could be anticipated from Fig. 2(b), $G_{\sigma\tau}$ depends very weakly on the density, whereas the other central components of G depend rather strongly on the local density at which the interaction is evaluated. In principle, this strong density dependence limits the validity of the LDA but this has not been investigated. With the exception of G_σ we see that below ~ 300 MeV, the HM86 values of $|G|$ at $k_F=0$ are in somewhat better agreement with the SP84 values than are the GPH values at $k_F=0.50$. This is particularly true in the isovector sector. Results using the free Paris t matrix (calculated independently but not shown) exhibit this same trend. The implications of some of the differences between the different forces in studying nucleon-nucleus scattering are discussed in Sec. III.

Figure 6 illustrates the energy and momentum-transfer (q) dependence of the HM86 interaction at intermediate energies at $k_F=1.1$ fm^{-1} corresponding to $\rho\approx 0.53$ normal density (ρ_0). With the exception of $G_{\sigma\tau}$ there is a rather strong energy dependence of the central parts of G. This is due to the large correlations present in G_0, G_σ, and G_τ which depend strongly on the collision energy. This strong energy dependence restricts the validity of the assumptions used in constructing the effective G-matrix interaction such as the procedures used to determine k_0 and K in terms of the incident and Fermi momenta and the single-particle potential. The energies quoted in Fig. 6 are the asymptotic laboratory energies of the incident nucleon. The relatively large isoscalar NN spin-orbit (LS) interaction depends weakly on the incident energy while the small isovector LS interaction de-

pends much more strongly on the energy. In the meson-exchange model this behavior may be understood in terms of the relatively large (small) bare potential associated with the exchange of σ and ω (ρ) mesons in the isoscalar (isovector) interaction. The higher-order terms (in V) are, therefore, relatively more important for G_τ^{LS}.

The energy and momentum dependence of the tensor parts of the effective G-matrix interaction are also illustrated in Fig. 6. Here the terms $G_0^{T'}$ and $G_\tau^{T'}$ are shown as a function of the exchange momentum transfer Q rather than for a fixed value of Q. In meson-exchange models,[20] the dominant part of the tensor force arises from the exchange of π and ρ mesons which each carry isospin 1. The small (isoscalar) G_0^T is consistent with this interpretation. In this same picture, the contributions $G_0^{T'}$ and $G_\tau^{T'}$ are believed to arise primarily from the large G_τ^T term acting in the exchange channel.[11,20] To the extent this is correct we find

$$[G_0^{T'}(Q)+G_\tau^{T'}(Q)\boldsymbol{\tau}_1\cdot\boldsymbol{\tau}_2]S_{12}(\hat{\mathbf{Q}})$$
$$\simeq -P_{12}G_\tau^T(q)S_{12}(\hat{q})\boldsymbol{\tau}_1\cdot\boldsymbol{\tau}_2$$
$$=(-\tfrac{3}{2}+\tfrac{1}{2}\boldsymbol{\tau}_1\cdot\boldsymbol{\tau}_2)G_\tau^T(Q)S_{12}(\hat{\mathbf{Q}})\ , \qquad (2.22)$$

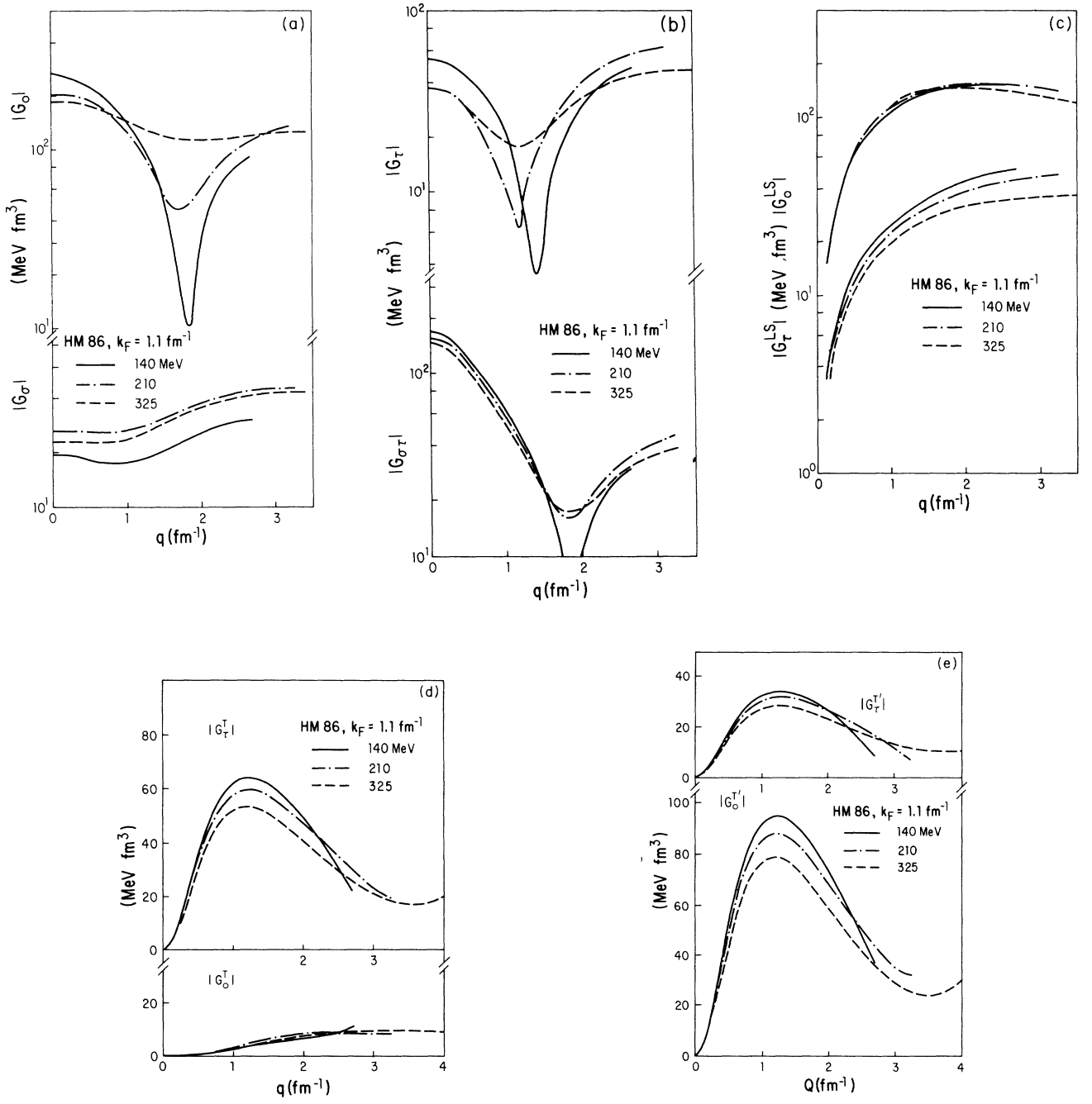

FIG. 6. Energy and momentum-transfer dependence of the HM86 interaction at $k_F = 1.1$ fm^{-1}.

where P_{12} denotes the Pauli exchange operator. Qualitatively, this assumption is borne out in that $|G_0^{T'}| \approx 3|G_\tau^{T'}|$. The direct and exchange momentum transfers are defined by Eq. (2.12). It has been shown[16] that the most important values of Q for nucleon-nucleus scattering are those near $Q=k_A$, where k_A is the momentum of the incident nucleon in the nucleon-nucleus system. These are essentially the values near the end points of the curves in Fig. 6. The peak value of G_τ^T is seen to change by less than 20% over the energy range considered. A similar energy dependence is also seen in $G_0^{T'}$ and $G_\tau^{T'}$ near the peaks.

Figure 7 displays the density and momentum-transfer dependence of the HM86 interaction for an incident proton energy of 210 MeV, an energy common to most intermediate energy facilities. The moduli of the different components of the force are shown for $k_F=0.0$, 1.1, and 1.36 fm^{-1} corresponding to densities of 0.0, 0.53, and 1.0 times normal density. Similar plots for the GPH interaction have been discussed by Kelly.[3] With the exception of $G_{\sigma\tau}$, each central term of the interaction is seen to depend rather strongly on density and exhibits a characteristic suppression at small q and, in the case of G_0, a modest enhancement at large q. These characteristics are examined in more detail in Fig. 8 where the real and imaginary parts of G_0 are shown separately. For the real part, $G_0(k_F=1.36)$ differs from $G_0(k_F=0)$ primarily by a decrease in attraction (or an increase in repulsion) of $\sim$20–25 MeV fm^3 roughly independent of q. The simple shift in ReG_0 with density reflects the dominant short-range character of the correlated (higher-order) terms in relating Re$G(\rho)$ to Re$G(\rho=0)$; see Eq. (2.15). Unlike the real part of G_0, Im$G_0(\rho)$ does not differ from Im$G_0(\rho=0)$ by a simple shift so that the additional correlation is going from $G(0)$ to $G(\rho)$ cannot be characterized as a zero-range correction. The Im$G(\rho)$ is better characterized by an overall suppression of Im$G(0)$ by a factor of $\sim$0.6 at this particular energy. This *suppression* can be understood in terms of Eq. (2.1) where the imaginary part of the G matrix is given by

$$\mathrm{Im}G(K,k,k_0)=-\bar{Q}(K,k_0)\int d\hat{\mathbf{k}}'\frac{k_0^2}{|\Delta|}V(\mathbf{k},\mathbf{k}'=k_0\hat{\mathbf{k}}')\,\mathrm{Re}G(K,\mathbf{k}',\mathbf{k}_0)+P\int d^3k'\frac{V(\mathbf{k},\mathbf{k}')\bar{Q}(K,k')\,\mathrm{Im}G(K,\mathbf{k}',\mathbf{k}_0)}{E(K,k')-E(K,k_0)}\ , \tag{2.23}$$

where Δ denotes the derivative of the energy denominator with respect to k' evaluated on the energy shell. As a first approximation, the G matrix in the right-hand side (rhs) of Eq. (2.23) may be replaced by the t matrix [see Eq. (2.15)]. Then the first term on the rhs of the above equation is proportional to the Pauli operator $\bar{Q}$ on the energy shell, while in the second term the Pauli operator enters as a part of the integrand. Therefore, for a component of the G-matrix interaction whose real part dominates (such as G_0), the imaginary part will be roughly proportional to the Pauli operator evaluated on the energy shell. The same observation holds if one iterates Eq. (2.23) to first order. The real part of the correlated part ($\tilde{G}$) of the G matrix, also obeys Eq. (2.23) with ImG and ReG being interchanged. Therefore, Re$\tilde{G}$ becomes proportional to $\bar{Q}(K,k_0)$ when ImG is the dominant part of the G matrix. Evaluation of $\bar{Q}$ in Eq. (2.4) at $k_F=1.36$ fm^{-1} and $T_L=210$ MeV gives the suppression factor of 0.6 mentioned above to within $\sim$10% at the on-shell point $k'=k_0$. The overall suppression of ImG_0 with increasing density was predicted qualitatively by Clementel and Villi.[21] As has been noted by Kelly and co-workers,[3] the large q enhancement in the modulus of G_0 is seen to arise from the ($\sim q$ independent) reduced attraction in ReG_0.

Above $\sim$100 MeV the density dependence of the spin-orbit and tensor parts of the interaction is relatively weak (but non-negligible) for $q \lesssim 1.5$ fm^{-1}. The main features of this density dependence may be understood in terms of the suppression of correlations with increasing density which are primarily important for large momentum transfers involving collisions at relatively short distances. The centrifugal barrier in $l>0$ states help shield these noncentral components from close encounters and, therefore, large correlations. A detailed analysis of short-range correlation effects on the G-matrix interaction (for the bound state problem) may be found in Refs. 11 and 12.

There has recently been considerable interest[22] in extracting and interpreting the longitudinal and transverse spin responses in nucleon-nucleus scattering. For this purpose, it is essential to know the relevant longitudinal and transverse spin couplings in the nuclear medium. Figure 9 shows the ratio of the transverse to longitudinal couplings as a function of momentum transfer at 325 MeV, a popular energy for investigating the nuclear spin response. The longitudinal V^l and transverse (V^t) couplings defined here include the central, tensor and spin-orbit contributions and are given by[23]

$$\begin{aligned} V^l(q)&=\eta E\ , \\ V^t(q)&=\frac{\eta}{\sqrt{2}}(C^2+B^2+F^2)^{1/2}\ , \end{aligned} \tag{2.24}$$

where η converts amplitudes to t matrices or G matrices as in Ref. 16, and C^2 stands for $|C|^2$, etc. These combinations reflect the interaction components relevant for calculating cross sections for unnatural parity excitations.[15,23,24] Both isoscalar and isovector coupling ratios are shown at zero and normal nuclear densities. The isoscalar coupling is seen to be predominantly transverse at all q shown, whereas the isovector coupling is largely transverse for $q \lesssim 1.25$ fm^{-1} and primarily longitudinal for larger q. The qualitative features of the couplings are rather insensitive to the local density. Quantitatively, the transverse dominance for $\Delta T=0$ is suppressed at full

density for small momentum transfers. The sharp peak in the $\Delta T=1$ coupling ratio near 0.7 fm^{-1} reflects a nearly complete cancellation of the $\Delta T=1$ central and tensor forces in V^l, a characteristic associated with OPE which has been pointed out earlier.[16] Analogous results at 210 MeV have the same qualitative features as those shown in Fig. 9 for 325 MeV.

III. SELECTED APPLICATIONS OF THE EFFECTIVE *G*-MATRIX INTERACTION

In this section we apply the effective interaction described above (henceforth denoted by HM86) to several transitions in nucleon-nucleus scattering which illustrate some of its properties which are relevant for exciting

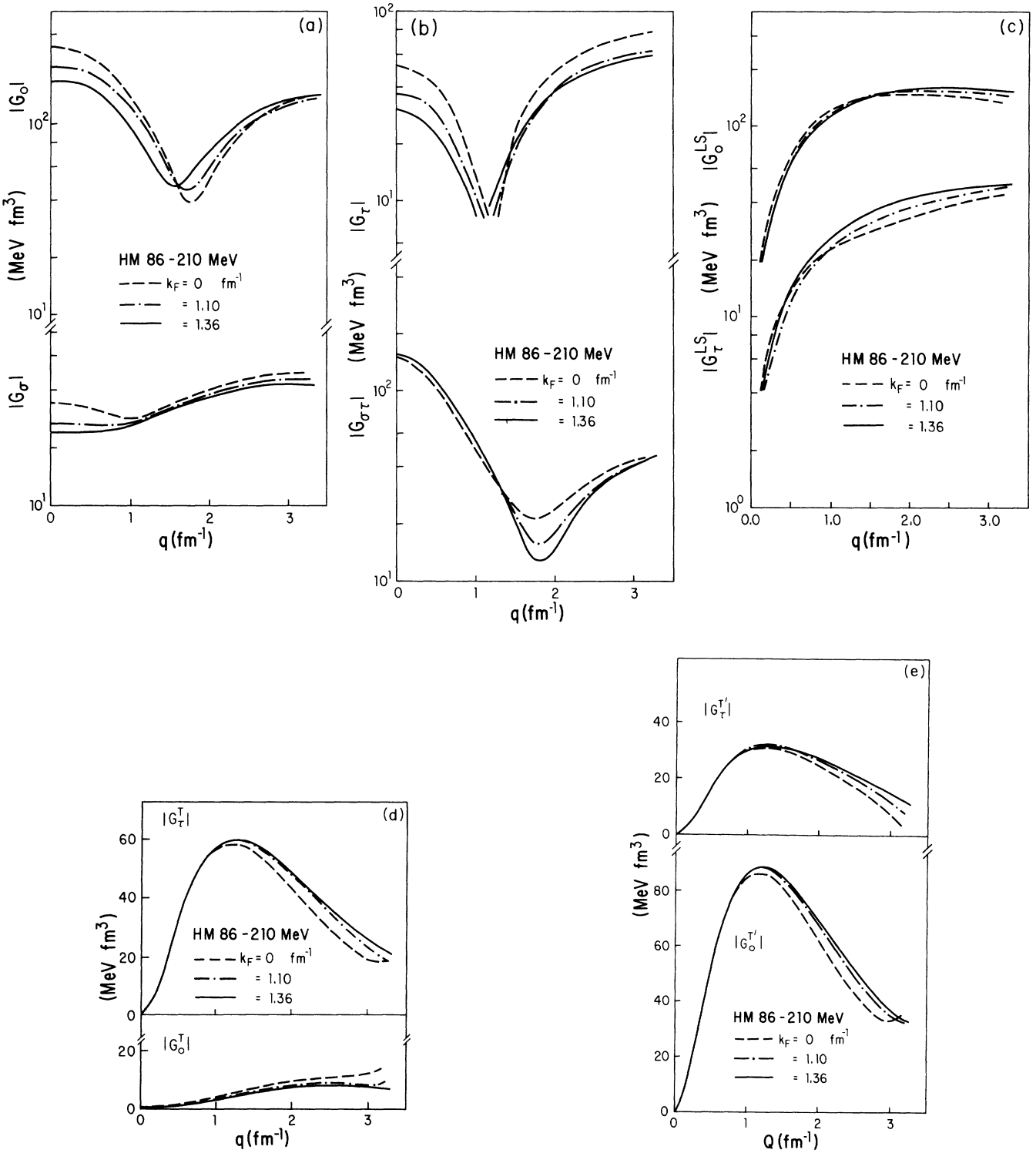

FIG. 7. Density and momentum-transfer dependence of the HM86 interaction at 210 MeV incident energy.

states requiring different spin and isospin transfers. Some of the remaining ambiguities and deficiencies in the interaction and its method of application are noted. Both direct and knock-on exchange terms are included in the calculations. For elastic scattering and natural parity excitations of angular momentum $J \leq 2$, the exchange terms are calculated in a well-established short-range approximation[16,25] for the local representation of the interaction considered here. The single-scattering approximation was used for the inelastic processes as well as for the optical potential for elastic scattering.

A. Elastic scattering

Medium corrections to the NN interaction are known[2,3] to be important for the calculation of optical potentials for use in the Schrödinger equation. Indeed, von Geramb and co-workers have obtained rather impressive results for elastic proton scattering from both light and heavy nuclei[2] using a G-matrix interaction (GPH) based on the Paris[5] potential. Here we consider the elastic scattering of protons from ^{90}Zr and ^{12}C at incident energies (T_L) of 121.5 and 200 MeV, respectively, using the effective G-matrix interaction (HM86) based on a one-boson-exchange version of the Bonn potential given in Table V of Ref. 4. The optical potential is calculated in a folded model and in each case the ground-state proton density used to construct the optical potential was taken to be consistent with electron scattering;[26] the neutron density was taken to be N/Z times the point proton density.

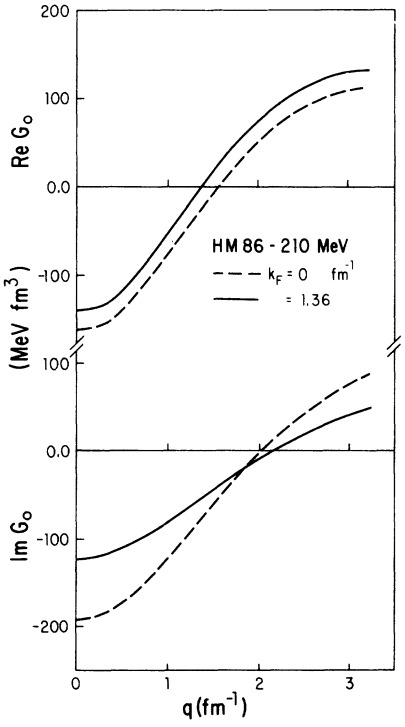

FIG. 8. Density and momentum-transfer dependence of the real and imaginary parts of the G_0 component of the HM86 interaction at 210 MeV.

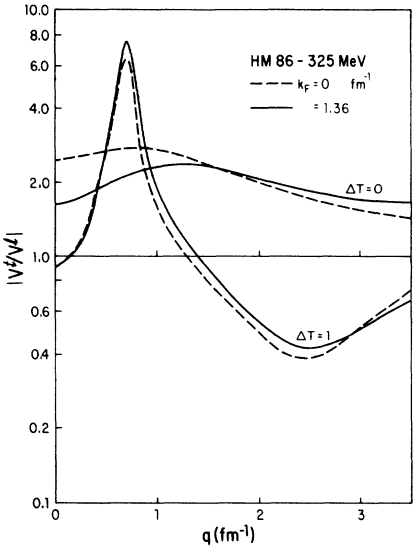

FIG. 9. Density and momentum-transfer dependence of the ratio of the transverse (V^t) to longitudinal (V^l) spin couplings at 325 MeV.

Measured[27] cross sections for $p + ^{90}$Zr elastic scattering are shown in Fig. 10 together with those calculated using the present effective interaction. The agreement is reasonable but not excellent. Curiously, the calculated cross section using a similar interaction based on an earlier version (HEA) (Refs. 13 and 28) of the Bonn potential

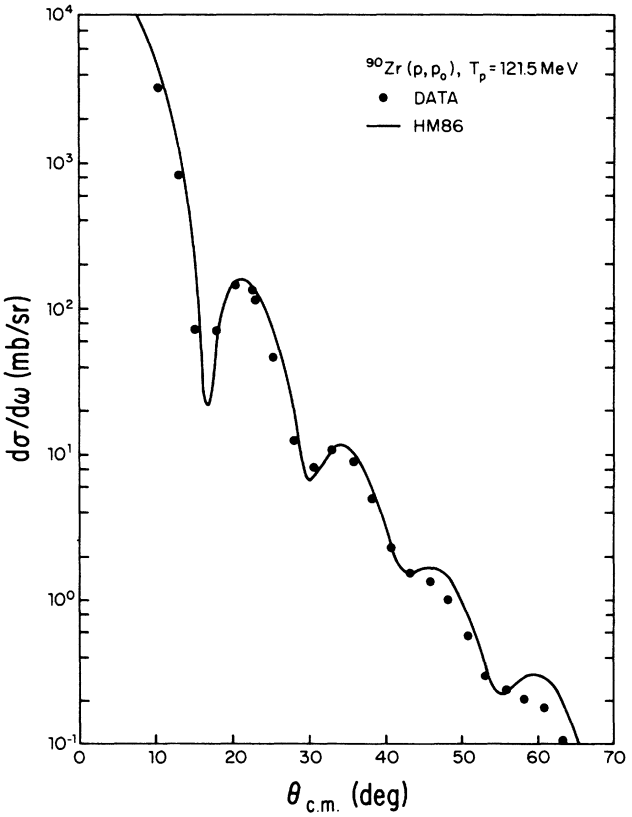

FIG. 10. Elastic $p + ^{90}$Zr scattering at 121.5 MeV. The solid curve corresponds to the use of a folded optical potential using the HM86 G-matrix interaction. The data are from Ref. 27.

agrees somewhat better with the data.

Figure 11 shows results for $p+{}^{12}C$ elastic scattering where cross section (σ) and analyzing power (A_y) data[29] are available. The solid curves were calculated using the HM86 interaction; the dashed curves were calculated using a free t-matrix interaction[16] based on the SP84 amplitudes of Ref. 19. The agreement between measured and calculated cross sections is quite reasonable when the density-dependent HM86 interaction is used and, as expected, represents a significant improvement over the results obtained using the SP84 interaction. An even more striking *improvement* is observed for A_y; however, even the G-matrix results are not in good agreement with the data.

B. Inelastic scattering and charge-exchange reactions

The observables for inelastic scattering and charge-exchange reactions were calculated in the distorted wave approximation using distorted waves calculated from either a *folded* model potential (F) or a purely *phenomenological* Woods-Saxon potential (P) as indicated.

1. The $^{12}C(p,p')$ reaction at 200 MeV

Excitations in ^{12}C provide a variety of different types of transitions which sample several symmetry and dynamical properties of *any* effective interaction. Moreover, electron scattering data are available for most of the transitions considered and this information is used to fix or constrain the p-shell transition densities of Cohen-Kurath[30] (CK) as described in Refs. 16 and 31. The (p,p') data are from Ref. 29.

Results for the excitation of the first 2^+ state at $E_x=4.44$ MeV are shown in Fig. 12. It is assumed that the excitation is purely scalar-isoscalar ($S=T=0$) in character and, therefore, samples the corresponding (density-dependent) part of the effective interaction; Coulomb excitation is included and a folded optical potential is used. The present calculation overestimates the

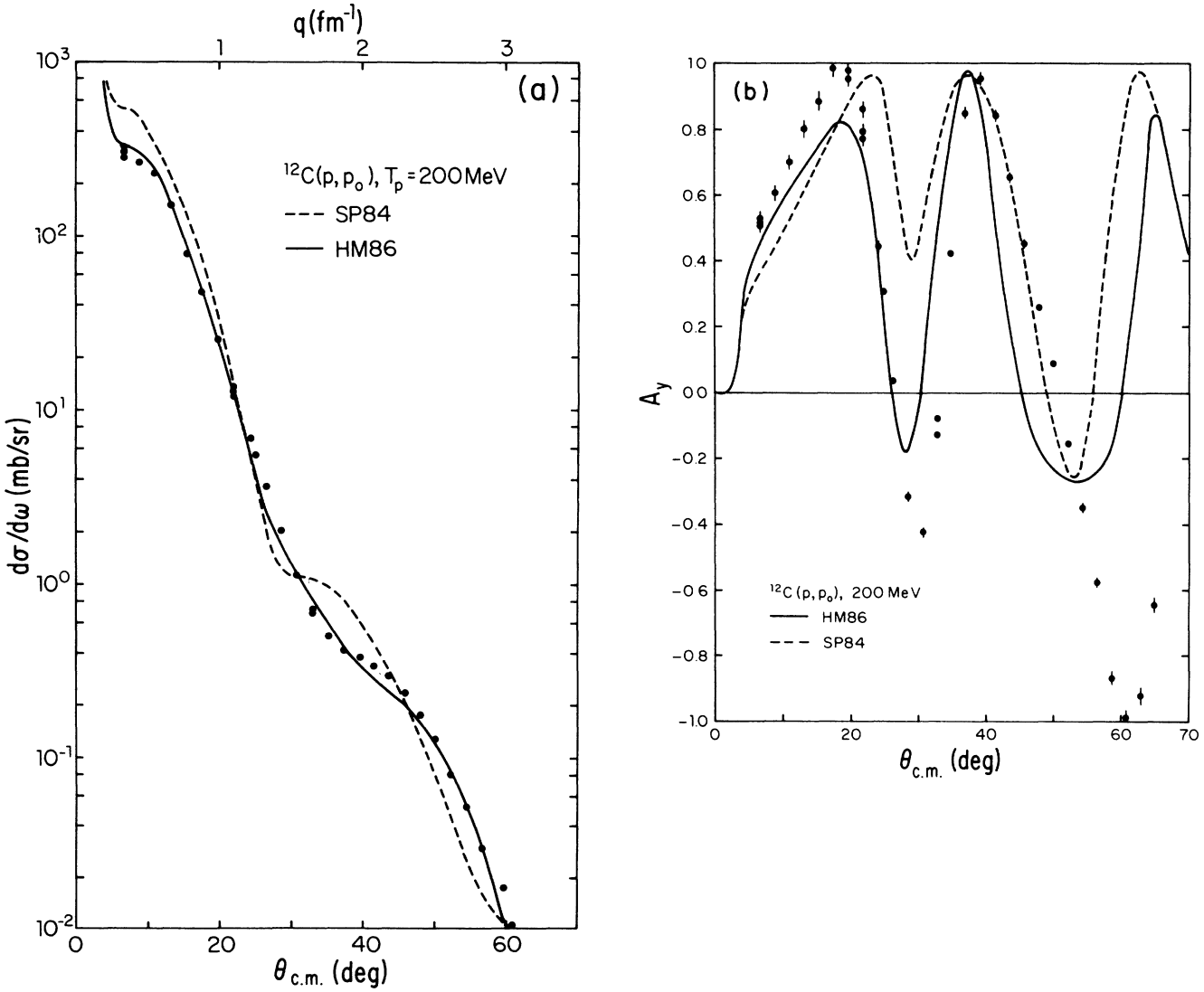

FIG. 11. Elastic $p+{}^{12}C$ scattering at 200 MeV. The dashed and solid curves were calculated using the SP84 and HM86 interactions described in the text. The σ and A_y data are from Ref. 29.

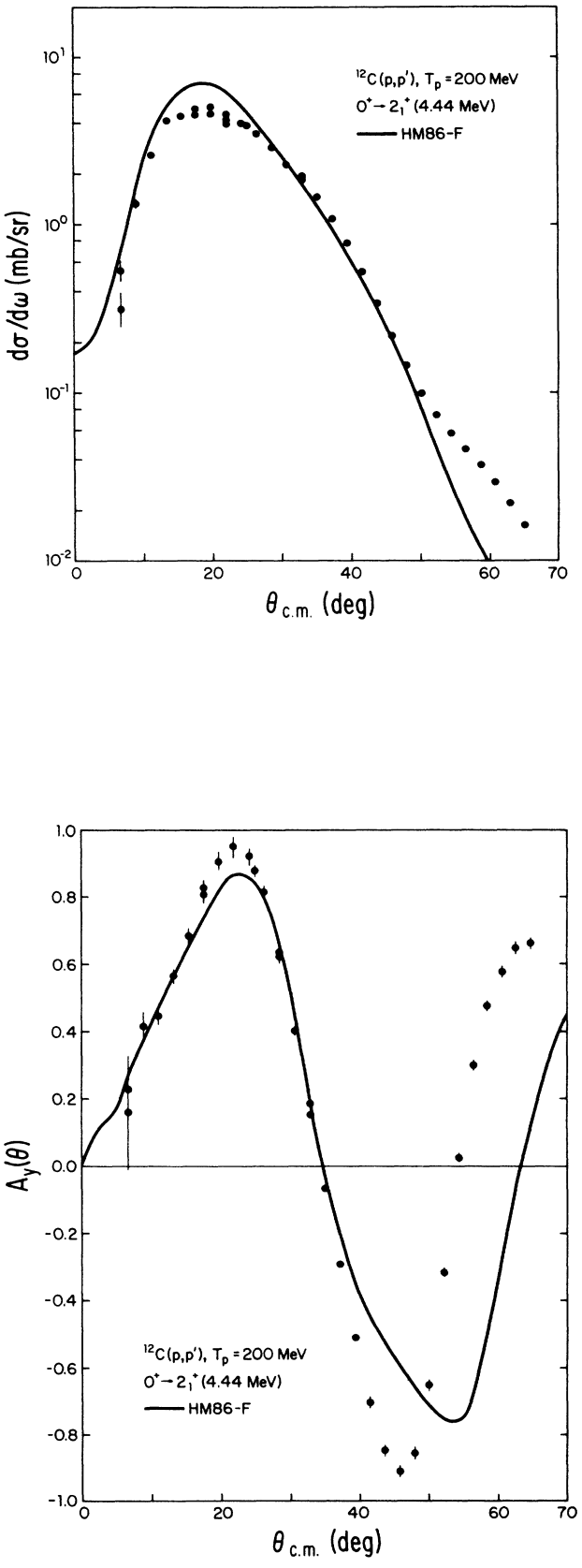

FIG. 12. Measured (Ref. 29) and calculated σ and A_y for the 2^+ (4.44 MeV) excitation in ^{12}C at 200 MeV incident energy. The HM86 interaction was used. F denotes the use of distorted waves derived from a folded optical potential.

cross section near its peak by $\sim 30\%$ as is the case[32] with the GPH interaction. This overestimate occurs *after* the CK transition density has been matched (in shape and magnitude) to the longitudinal (e,e') form factor out to ~ 2 fm^{-1} ($\sim 45°$ at 200 MeV) and therefore suggests that the HM86 interaction is too large at small q. A_y is described reasonably well for $\theta_{c.m.} \leq 40°$. Although far from perfect, the HM86 results represent a considerable improvement over those obtained using the free t-matrix interaction with phenomenological distorted waves such as shown in Ref. 29.

Figure 13 shows measured and calculated cross sections and analyzing powers for excitation of the 0_2^+ state at 7.65 MeV. The transition density, which in this case is taken from Ref. 33, has a node near 2.5 fm which makes this excitation somewhat more sensitive to density-dependence in the NN interaction than more surface-peaked transitions. Folded distorted waves using the full density-dependent HM86 interaction were used in each calculation shown. The dashed curves correspond to the use of only the zero-density G matrix $[G(0)]$ in the *transition* potential, whereas the solid curves correspond to the use of the full density-dependent $G(\rho)$. For $\theta_{c.m.} < 30°$ the full density-dependent calculations are in significantly better agreement with the data than are the results using $G(0)$. However, as in the case of the 2^+ state at $E_x = 4.44$ MeV, G_0 appears to be too large at small momentum transfers. The curve denoted by $G + \delta G$ corresponds to including the correction suggested by Cheon[34] for $S = T = 0$ collective excitations. The amount of improvement in the calculated cross section is similar to that achieved in going from $G(0)$ to $G(\rho)$. It is not clear that the Cheon correction improves the agreement between measured and calculated A_y. Similar, but smaller effects occur when δG is included in the 2_1^+ excitation. Even with these corrections, the calculated peak cross sections for the 0_2^+ and 2_1^+ transitions need to be multiplied by ~ 0.7 in order to agree with the data at this energy.

Measured and calculated results for excitation of the 1^+, $T=0$ state at an excitation energy (E_x) of 12.71 MeV are shown in Fig. 14. The wave functions are those of Cohen and Kurath.[30] Because of the strong sensitivity of (e,e') scattering to isospin mixing, electron scattering provides little help in pinning down those parts of the transition density most relevant for (p,p'). Moreover, distorted wave calculations have been typically unsuccessful in describing this transition for $T_L \leq 200$ MeV; the CK wave functions do provide a reasonable description of the (p,p') data for $T_L \geq 400$ MeV.[16] As in the case of calculations[29] using the free t matrix, the present interaction yields a poor description of the cross section data. Both interactions yield cross sections which are too large and which lack the observed structure. Nevertheless, a reasonable description of the analyzing power is obtained at this energy where the central, spin-orbit and tensor parts of the interaction each contributes significantly. The level of agreement between the measured and calculated observables is quite similar to that obtained using free t-matrix interactions.[16,29] The result for the cross section seems to indicate that the isoscalar tensor force G_0^T

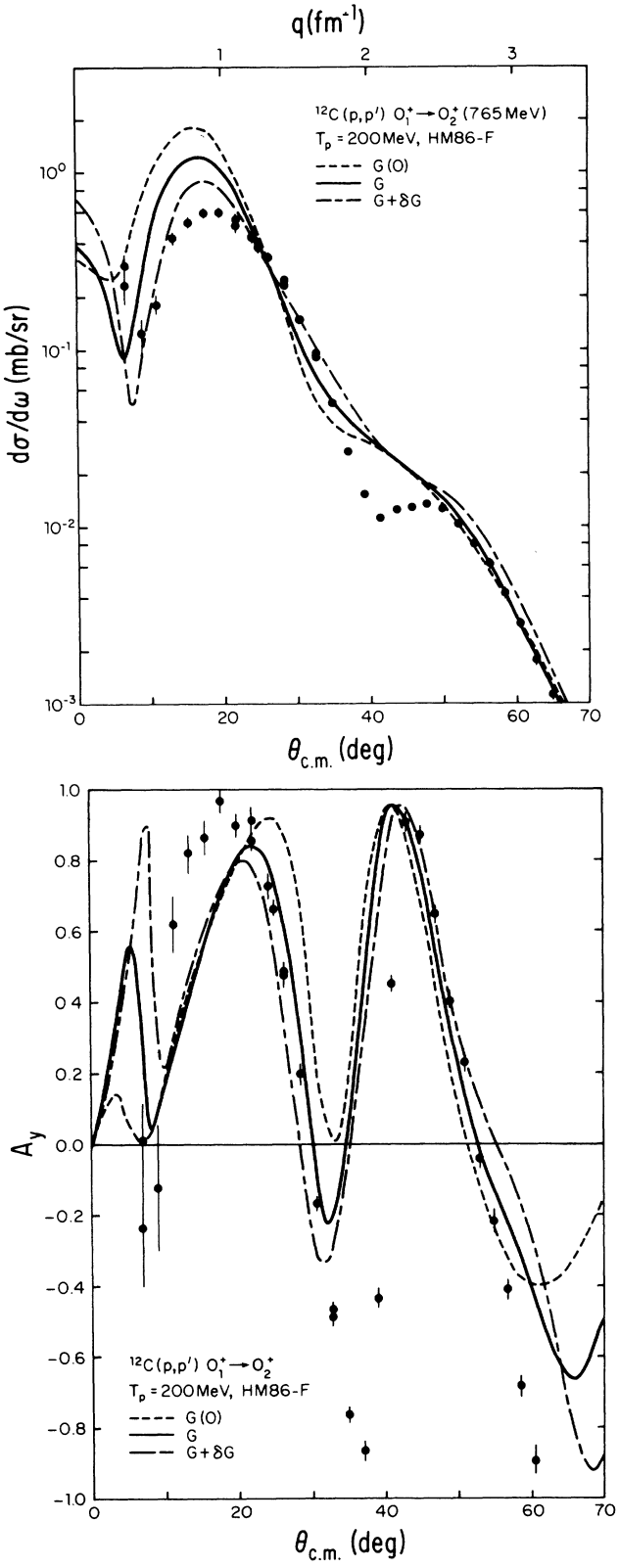

FIG. 13. Measured (Ref. 29) and calculated σ and A_y for the 0^+ (7.65 MeV) excitation in ^{12}C at $T_L = 200$ MeV. The same folding-model distorted waves were used for each calculation. The dashed (solid) curve denotes the use of the zero-density (full) G-matrix transition operator. The long-dashed–short-dashed curve includes δG, the Cheon correction to the full G-matrix interaction described in the text.

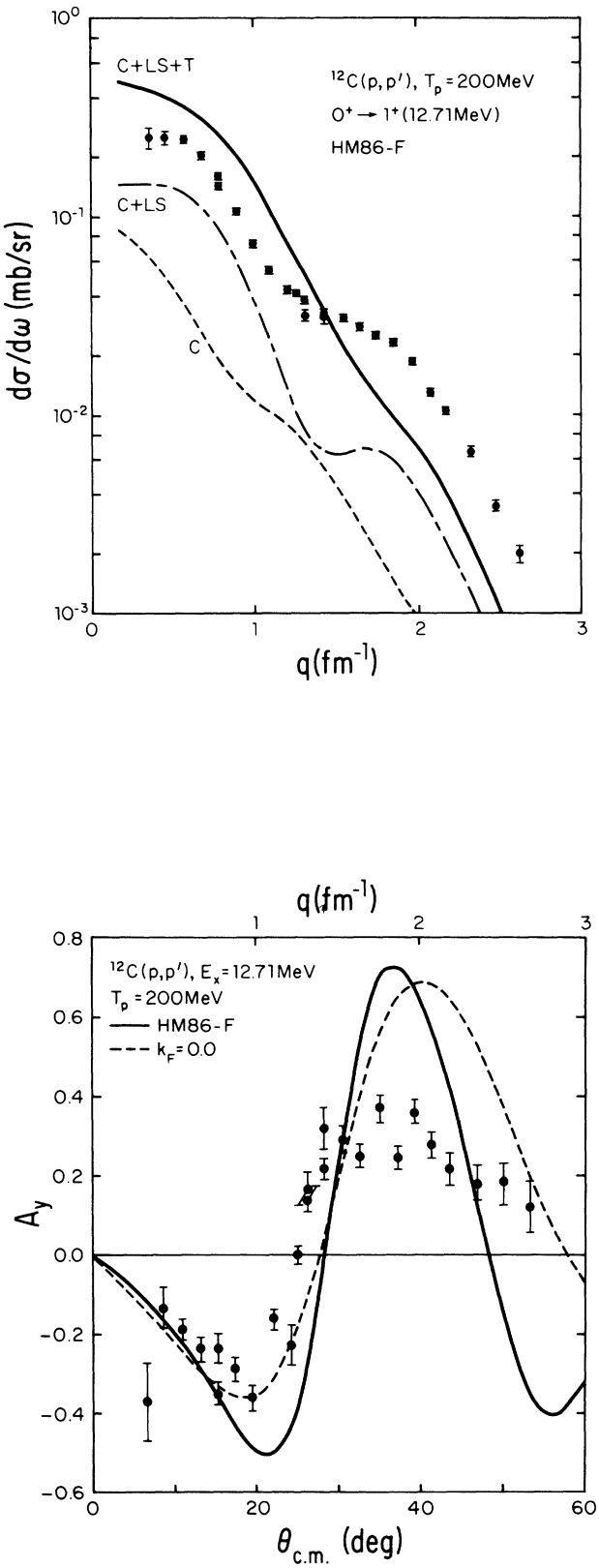

FIG. 14. Measured (Ref. 29) and calculated observables for the 1^+ (12.71 MeV) excitation in ^{12}C at $T_L = 200$ MeV. C, LS, and T denote contributions from the central, spin-orbit, and tensor parts of the HM86 interaction. For $A_y(\theta)$, the dashed (solid) curves denote the use of the zero-density (full) HM86 interaction.

is too strong at large exchange momenta Q. We observe that this part of the force is basically the Pauli exchange term arising from the strong *isovector* tensor component G_τ^T [see Eq. (2.22)]. Figure 14 shows that the $k_F=0$ effective G-matrix interaction yields $A_y(\theta)$ qualitatively similar to that obtained using the full density-dependent interaction $[G(\rho)]$. The calculated cross section using the $k_F=0$ interaction is $\sim 50\%$ larger than that shown in Fig. 14; the shape is similar to that shown.

Results for the excitation of the 1^+, $T=1$ state at $E_x=15.11$ MeV are shown in Fig. 15. The CK wave functions are in agreement with the relevant Gamow-Teller matrix element measured in the $A=12$ system; moreover, the shape and magnitude of the corresponding (e,e') form factor is reasonably well described[29] by these wave functions for $q \lesssim 1$ fm^{-1}. As for the 12.71 MeV excitation, the cross sections corresponding to the central, central plus spin orbit (LS), and central plus LS plus tensor parts of the interaction are shown. The isovector LS part of the NN interaction is seen to be especially weak for $q \lesssim 1.5$ fm^{-1}; the isovector tensor force is seen to be important for $q \geq 0.25$ fm^{-1}. The complete calculated cross section is in good agreement with the data for $q \lesssim 1$ fm^{-1}, where the transition density is most reliable. Moreover, the minimum near $q=1.25$ fm^{-1} is better described using the present interaction than the SP84 interaction.[15] Although the calculated A_y is in rather poor agreement with the data, results obtained[15] using the SP84 interaction hardly resemble the data at all. Overall, the agreement with the cross-section data is reasonable where the wave functions are most definitive. As noted earlier, the density dependence is weak for this type $(S=T=1)$ of transition.

Measured and calculated cross sections and analyzing powers for excitation of the 2^+, $T=1$ state at $E_x=16.11$ MeV are shown in Fig. 16. The $S=0$ and $S=1$ CK transition densities were reduced as in Ref. 31 so as to agree with (e,e') results for this excitation. Additional reduction of the calculated cross section by $\sim 25\%$ would yield a much better description of the data for $1 \lesssim q\,(\text{fm}^{-1}) \lesssim 2$. This transition, dominated by the tensor force, suggests that the strength of the isovector part of the NN tensor force may be too large by $\sim 10\%$. Calculations for $T_L \gtrsim 200$ MeV using t-matrix interactions also overestimate the cross section for this transition by similar amounts. The results for A_y shown in Fig. 16 also suggest that the tensor force may be too large. We should emphasize that we have used folding-model distorted waves and have not studied ambiguities arising from the use of different optical potentials.

2. The $^{48}Ca(p,n)^{48}Sc$ (IAS) transition at 134 MeV

Results for the excitation of the isobaric analogue state (IAS) in the ^{48}Ca(p,n) reaction are shown in Fig. 17 for cross section and A_y data.[35] Each calculation was made using distorted waves generated by a folded optical potential based on the full density-dependent interaction. As is usual, the transition to the IAS was assumed to exhaust the Fermi strength from the ground state. The solid (dashed) curve corresponds to the use of the full

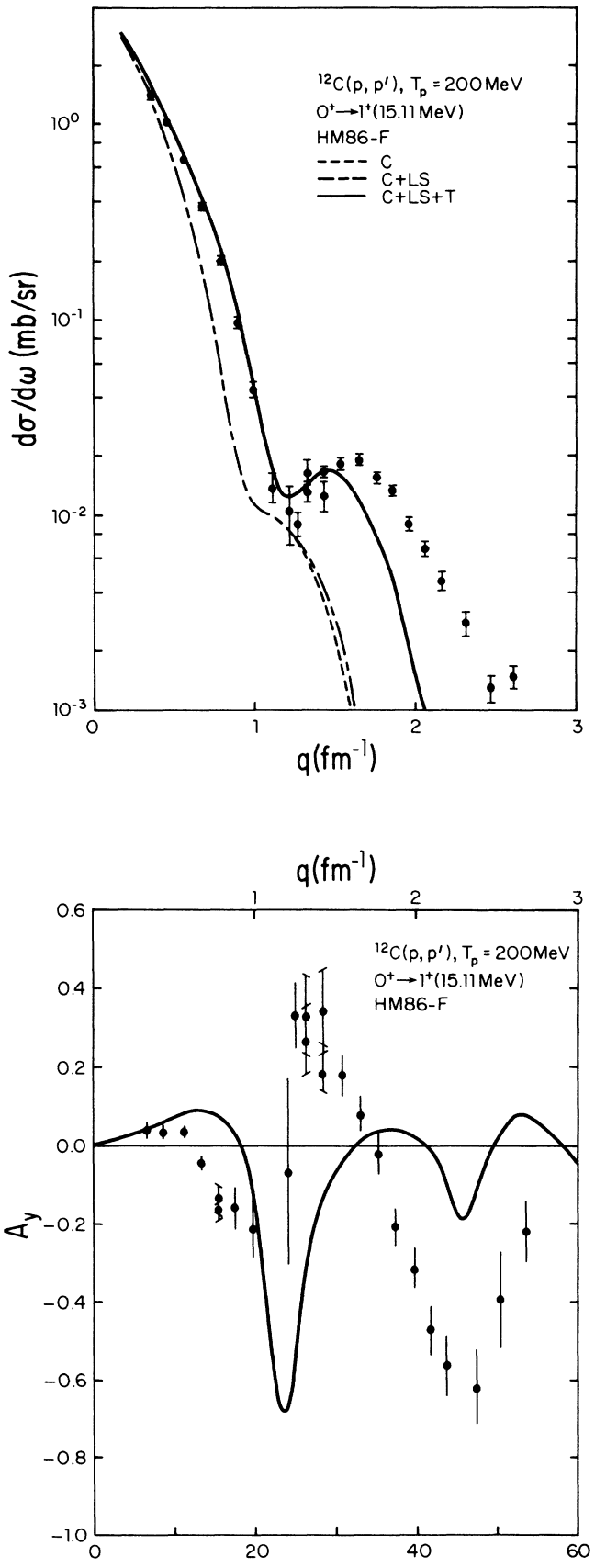

FIG. 15. Measured (Ref. 29) and calculated observables for the 1^+ (15.11 MeV) excitation in ^{12}C at $T_L=200$ MeV. The notation is as in Fig. 14.

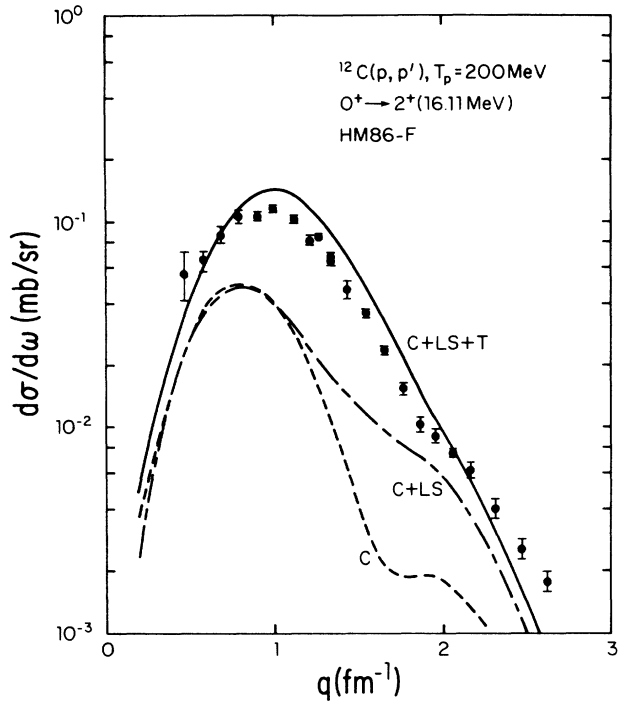

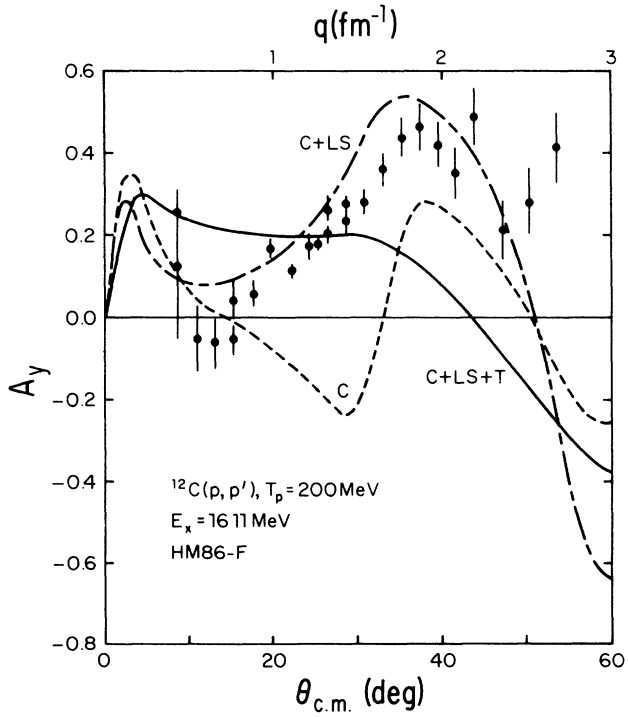

FIG. 16. Measured (Ref. 29) and calculated observables for the 2^+ (16.11 MeV) excitation in ^{12}C at $T_L=200$ MeV. *C*, *LS*, and *T* are as defined in Fig. 14.

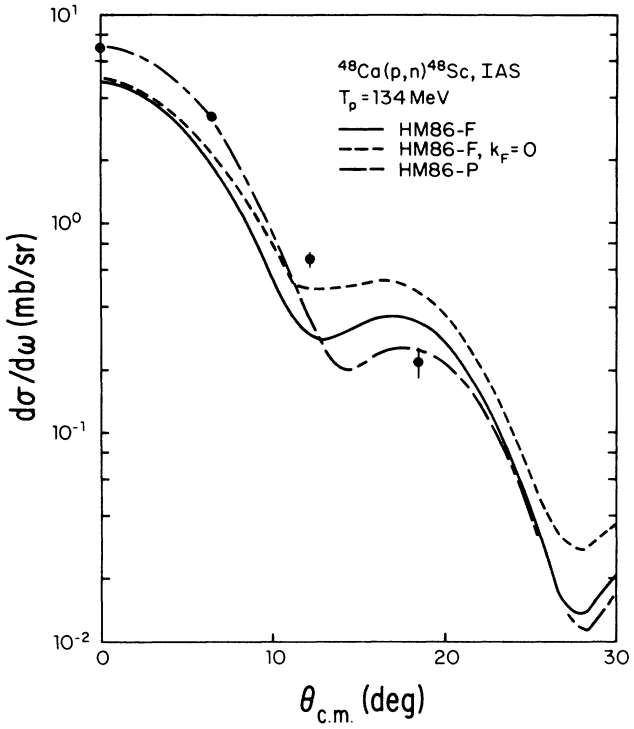

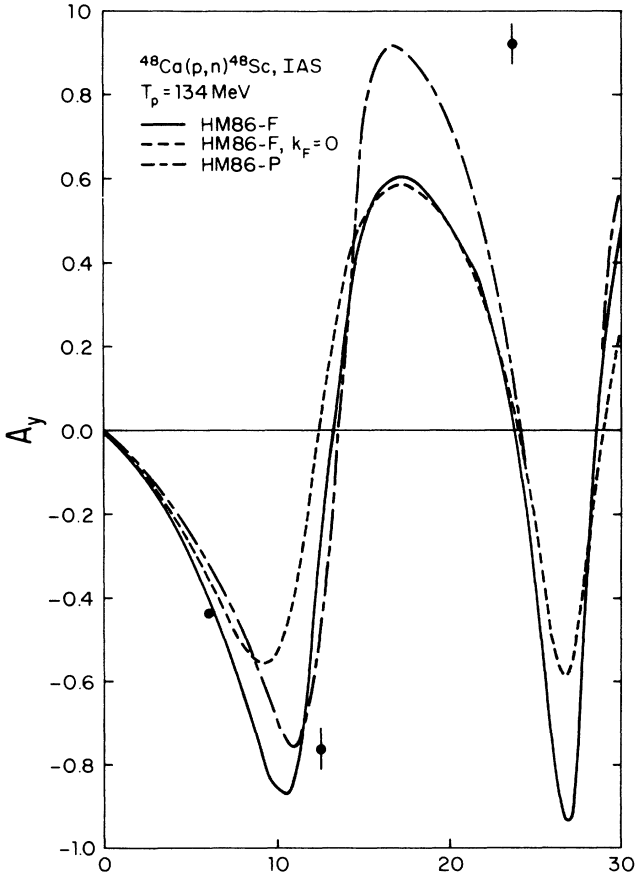

FIG. 17. Measured (Ref. 35) and calculated charge-exchange observables for the ^{48}Ca(p,n) reaction at $T_L=134$ MeV. $F(P)$ denotes the use of folding-model (phenomenological) distorted waves and $k_F=0$ denotes the use of the zero-density HM86 transition operator.

(zero-density) HM86 interaction. Although the use of the full density-dependent interaction improves the agreement for A_y, it slightly worsens the agreement between measured and calculated cross sections. The smaller cross section obtained in the case of full HM86 interaction as compared to the zero-density case arises from the decrease in $|G_\tau|$ with increasing density (see Figs. 5 and 7). A renormalization of the calculated cross section by ~ 1.4 is needed to describe the data at small angles. Such monopole transitions in medium to heavy mass nuclei have been shown[15] to be especially sensitive to the distorting potential. In particular, folded optical potentials typically yield[15,28,36] cross sections which are considerably smaller than those predicted using phenomenological optical potentials which describe elastic scattering. The use of folded potentials also suppresses the role of density dependence in the transition operator (here G_τ). Results of calculations using phenomenological distorted waves with the full, density-dependent interaction as the transition operator are also shown in Fig. 17. This agreement with the forward-angle cross section is excellent without any renormalization which implies that the zero-density interaction will overestimate the data. The results for A_y are less definitive.

3. *The $^{14}C(p,n)^{14}N$ reaction at 0°*

Figure 18 shows the energy dependence of measured and calculated ratios of cross sections for exciting the isobaric analog (Fermi) state at $E_x = 2.31$ MeV and the pure Gamow-Teller (GT) state at $E_x = 3.95$ MeV. Both Fermi and GT matrix elements are known[37] for these transitions. Calculations were made using effective G-matrix interactions based on the Bonn and Paris potentials as well as the SP84 t-matrix interaction. The differences in the ratios using the three interactions may be ascribed primarily, though not entirely, to differences in the calculated IAS cross sections which are driven primarily by the G_τ part of the interaction (see Fig. 5). The effects of using different types of distortion on the cross section *ratios* are very small. Overall, the HM86 interaction provides the best description of the measured[36,38] ratios.

4. *Excitation of high-spin stretched states*

Stretched excitations in nuclei provide some of the most definitive tests[39] of the NN interaction at large momentum transfers. These unnatural parity excitations involve only one particle-hole (p-h) component, and a single-orbital angular-momentum transfer $L = J - 1$, where J is the total angular-momentum transfer and $J = j_p + j_h$. It has been shown elsewhere[39] that isovector stretched states are populated primarily by the large isovector tensor force, whereas for isoscalar stretched states both spin-orbit and tensor forces contribute significantly.

We consider the excitation of the $T=0$ and $T=1$, 6^- stretched states in the $^{28}Si(p,p')$ reaction at 134 MeV. Comparisons between measured and calculated cross sections and A_y are shown in Fig. 19(a). The particle-hole configuration here is $(f_{7/2}, d_{5/2}^{-1})$ and the oscillator parameters were chosen following Hintz *et al.*[39] F denotes the use of a folded optical potential. The calculated cross sections for the $T=1$ state have been multiplied by 0.31 as is required by (e,e') data. The agreement between measured and calculated cross sections and A_y is quite reasonable for this transition, suggesting that the strength of the isovector tensor force is quite reasonable. The strong similarity between the solid curve $[G(\rho)]$ and the one with $k_F = 0$ illustrates the rather small medium corrections to the isovector part of the tensor force. This

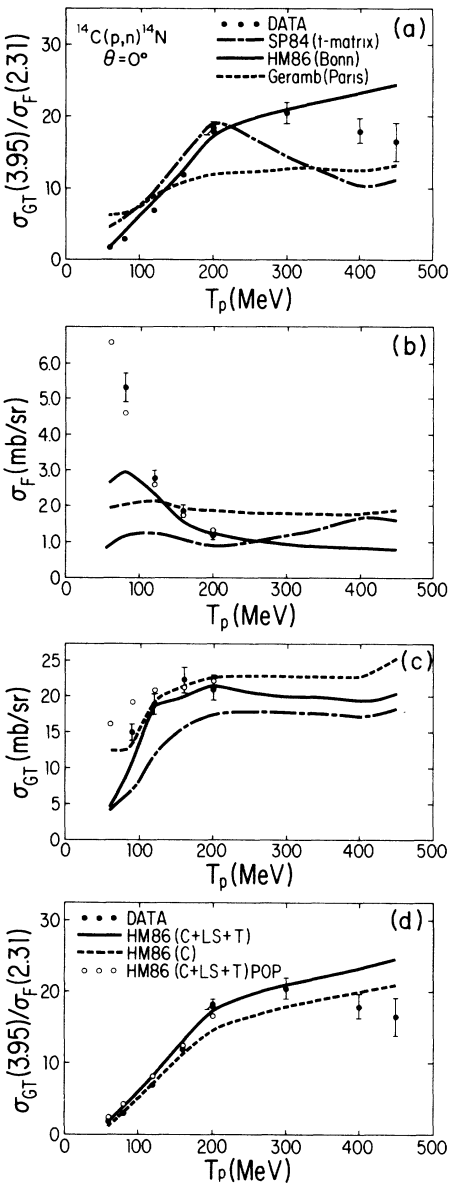

FIG. 18. (a) Measured and calculated ratios of the 0° cross sections for GT and Fermi transitions in the reaction $^{14}C(p,n)$. (b) Measured and calculated values of the 0° Fermi cross sections for the reaction $^{14}C(p,n)$. The curves (open circles) correspond to the use of folded (phenomenological) optical potentials (POP). (c) Measured and calculated values of the 0° GT cross sections for the reaction $^{14}C(p,n)$. (d) Measured and calculated values of 0° cross section ratios for the $^{14}C(p,n)$ reaction. C, LS, and T denote central, spin-orbit, and tensor parts of the NN force.

confirms our expectations based on the strong one-pion-exchange contribution to this part of the force. The good agreement for this transition appears to be inconsistent (quantitatively) with the results discussed earlier for the isovector 2^+ excitation in ^{12}C at 16.1 MeV. However, it should be noted that the 6^- stretched configuration is believed to be simpler than the 2^+ excitation in ^{12}C in that only an $S=1$ transition density enters the 6^- excitation. We have verified that the cross section for the excitation of this 6^- state in ^{28}Si is also well described at 180 MeV,[39] with the same renormalization of the particle-hole strength. This latter result indicates that the noted inconsistency is unlikely due to the consideration of somewhat different incident energies for the two transitions.

For the $T=0$ excitation in ^{28}Si, the shapes of the measured and calculated observables are in good agreement as shown in Fig. 19(b). In this case, however, the calculated (p,p') cross section with unit p-h strength has to be multiplied by $N=0.17$ to agree with the data. Similar calculations for the (π,π') reaction require $N=0.11$.[39] Calculations by Hintz *et al.*[39] for this same (p,p') transition using the SP84 t-matrix interaction and a phenomenological optical potential require $N=0.12$. As in the

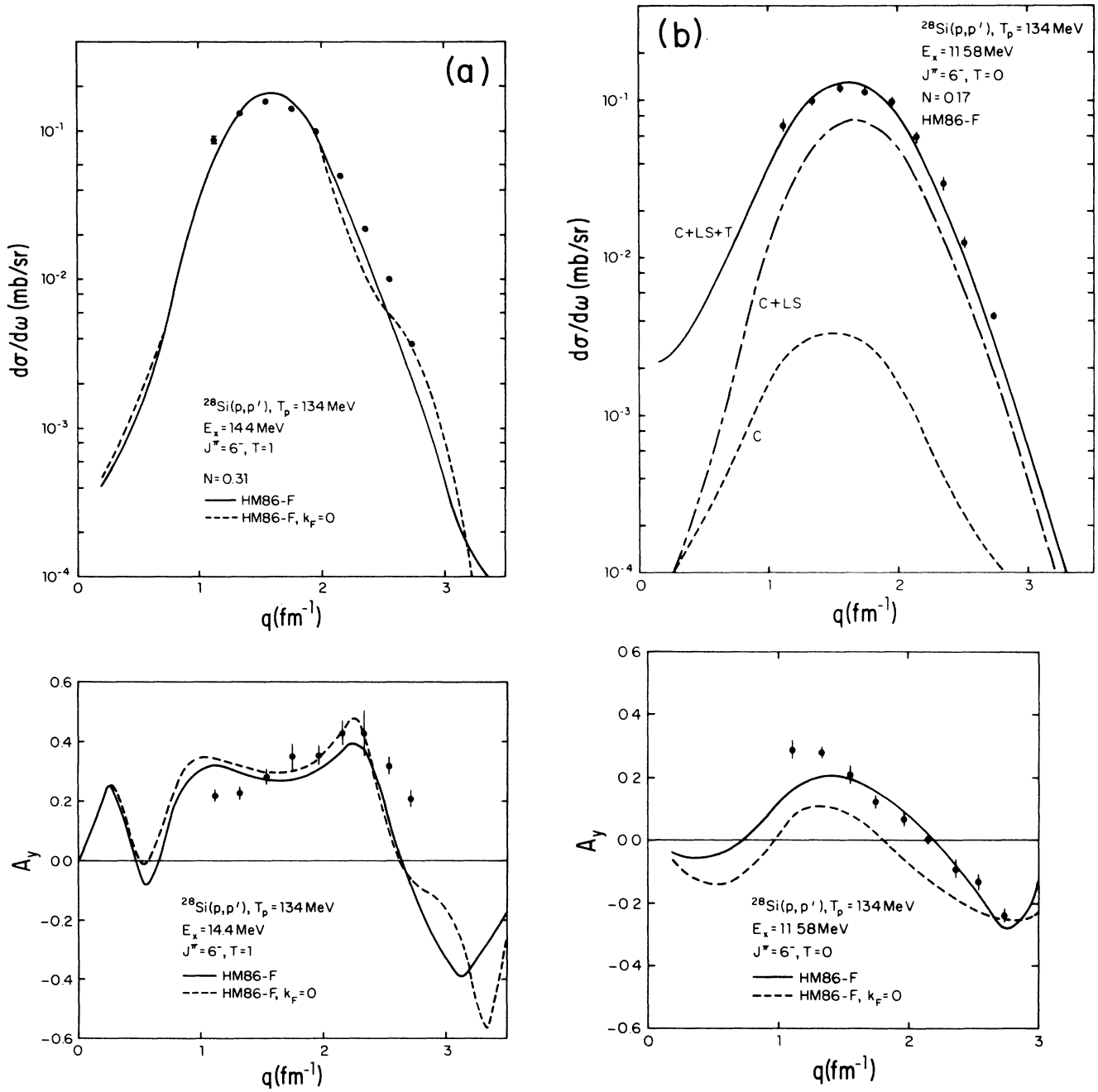

FIG. 19. (a) Measured (Ref. 39) and calculated observables for the $6^-(T=1)$ excitation in ^{28}Si at $T_p=134$ MeV. The solid and dashed curves have the same meaning as in Fig. 17. (b) Same as (a) for the $6^-(T=0)$ excitation in ^{28}Si at $T_p=134$ MeV; the C, LS, and T curves are as in Fig. 14.

case of the $T=1$ excitation, density-dependent effects on the calculated *cross section* are very weak (not shown). However, as seen in Fig. 19(b), the agreement between measured and calculated $A_y(\theta)$ is improved significantly when the full density-dependent interaction is used.

IV. SUMMARY

A local density-dependent *NN* interaction (HM86) based on one of the recently published OBEP versions of the Bonn potential has been derived from the Bethe-Goldstone equation for the *G* matrix in nuclear matter for use in calculations of nucleon-nucleus scattering between 50 and 450 MeV incident energies. The validity of the *G*-matrix interaction approach is expected to depend on the projectile's incident energy. In particular, at the lower energies where the incident momentum is comparable to the Fermi momentum, the validity of the *G*-matrix approach is highly questionable since other types of correlations, not taken into account by the *G*-matrix, become very important. Above the threshold for pion production we have not included any inelasticity. Many of the methods and approximations used to construct the *NN* interaction are given in this work or in Refs. 11 and 16. As in Ref. 16, we have parametrized the interaction at several particular energies and densities in a way to make it relatively convenient to use in some of the most widely used proton scattering programs [DWBA-70 (Ref. 40) and its offspring, and ALLWORLD (Ref. 41)] at intermediate energies. Medium corrections arising from Pauli blocking and the (self-consistent) single-particle potential have been included in a way which makes the connection with *NN* scattering relatively transparent.

Some of the dynamical aspects of the different parts of the *G*-matrix interaction have been displayed and discussed. In particular, we have considered the energy, density, and momentum transfer dependence of the interaction in anticipation of its application to *N*-nucleus scattering. Although our emphasis here is not on detailed analyses of specific measurements of nucleon-nucleus scattering observables, we have applied the interaction to a variety of transitions, primarily in the 100–200 MeV range of energy, which illustrate some of its merits and weaknesses. Particular emphasis has been placed on the relative importance of medium corrections in the different terms of the interaction and their implication for cross sections and spin observables in transitions which are selectively sensitive to these different terms. For elastic scattering and the excitation of $S=T=0$ collective states, the full density-dependent results are systematically in better agreement with the data than are calculations using either the zero-density HM86 interaction or the SP84 *t*-matrix interaction. Even so, the inelastic cross sections of this type are still overestimated by $\sim 30\%$ when the density-dependent *G*-matrix is used. One possible resolution of this problem may be the explicit inclusion of relativistic dynamical effects which have been shown to reduce the attraction of G_0 at small q.[42] Results for excitations involving spin and/or isospin transfer $\neq 0$ tend to be less definitive with regard to the need for density dependence. The ratios of isovector 1^+ to isovector 0^+ cross sections in the $^{14}C(p,n)$ reaction are consistent with a relatively strong density-dependent G_τ together with a nearly density-independent $G_{\sigma\tau}$. As with free *t*-matrix interactions, the largest discrepancies between the measured and calculated observables occur for isoscalar, $S=1$ excitations where the exchange contributions associated with the tensor force are large.

Finally, we hope that a clearer and more definitive pattern of the deficiencies of the effective *G*-matrix interaction will emerge following a more systematic and detailed application of it over a much wider range of energies than has been attempted here. The range and strength parameters of the interaction are available from the authors upon request at energies between 50 and 425 MeV.[43] On the more theoretical side, we must work towards treating the off-shell and nonlocal behaviors of the *G*-matrix carefully and perhaps improve the way in which the local density approximation is implemented as well as study its domain of validity.

ACKNOWLEDGMENTS

We are pleased to thank J. A. Carr, F. Petrovich, and J. J. Kelly for the use of their code ALLWORLD, M. A. Franey for his help with some of the scattering calculations, and K. Holinde and R. Machleidt for providing the OBEP code. The authors also appreciate the support of the Institut für Kernphysik, KFA, Jülich in the preliminary stages of this work. This work was supported in part by National Science Foundation, Grants PHY-8519653, PHY-8542806, and PHY-8607684.

APPENDIX

In the present work, we have derived a *G*-matrix interaction for use in calculations of elastic and inelastic nucleon scattering using the one-boson-exchange (OBE) version of the Bonn potential.[4] The OBEP developed by the Bonn group is actually a relativistic potential. The use of such a potential in a nonrelativistic BG equation involves approximations which merit some discussion. We first outline the derivation of the scattering equation in which the OBEP has been used (and determined).

The scattering amplitude is obtained in the framework of a three-dimensional reduction of the Bethe-Salpeter equation[44] which for the two-fermion invariant scattering amplitude is written schematically as

$$\hat{T}=\hat{K}+i\int \hat{K}\hat{g}\hat{T}\ , \tag{A1}$$

where $\hat{K}$ denotes the irreducible interaction kernel with respect to the two single-fermion lines and $\hat{g}$ is the relativistic two-fermion propagator. The three-dimensional reduction of Eq. (A1) is achieved by first rewriting Eq. (A1) in terms of two coupled equations

$$\hat{T}=\hat{U}+\int \hat{U}\hat{g}\hat{T}\ , \tag{A2a}$$

$$\hat{U}=\hat{K}+\int \hat{K}(i\hat{g}-\hat{g})\hat{U}\ . \tag{A2b}$$

The two-fermion propagator $\hat{g}$ is chosen such that it

preserves the covariant form of Eq. (A2a) and ensures that the resulting scattering amplitude $\hat{T}$ satisfies the relativistic unitarity relation. Moreover, if $\hat{g}$ is a "good approximation" to $i\hat{Q}$, the quasipotential $\hat{U}$ defined in Eq. (A2b) may be calculated in perturbation theory. In particular, one might keep only the lowest-order terms, i.e., $\hat{U}\simeq\hat{K}$, where in the present work the interaction kernel $\hat{K}$ is assumed to be given by the OBEP $\hat{V}$.

The two-fermion propagator $\hat{g}$ is not unique and a number of different choices have been proposed.[45–47] Among these, the most common one and the one which we are interested in here is that of Blankenbecler and Sugar[45] which, using the notation of Bjorken and Drell,[48] is

$$g_{\rm BBS}(\mathbf{K},k'_\mu;\omega)=-\int_{4m^2}^{\infty}\frac{d\omega'}{\omega'-\omega-i\eta}(\not{p}'_{1\mu}+m)(\not{p}'_{2\mu}+m)\delta(p'^2_{1\mu}-m^2)\delta(p'^2_{2\mu}-m^2)\ . \tag{A3}$$

Here, ω denotes the Lorentz invariant defined by

$$\omega\equiv 4K_\mu K^\mu=(E_{p_1}+E_{p_2})^2-4K^2\ , \tag{A4}$$

with $E_p=(\mathbf{p}^2+m^2)^{1/2}$ and $\mathbf{K}$ defined by Eq. (2.2); k_μ is the four vector defined by

$$k_\mu=\frac{p_{1\mu}-p_{2\mu}}{2}\ . \tag{A5}$$

The integration over ω' can be carried out giving

$$\begin{aligned}g_{\rm BBS}(\mathbf{K},k'_\mu;\omega)&=-4m^2\left[\frac{E_{p'_1}+E_{p'_2}}{2E_{p'_1}E_{p'_2}}\right]\frac{\Lambda_+(\mathbf{p}'_1)\Lambda_+(\mathbf{p}'_2)}{(E_{p'_1}+E_{p'_2})^2-4\mathbf{K}^2-\omega-i\eta}\delta\left[k'_0-\left[\frac{E_{p'_1}-E_{p'_2}}{2}\right]\right]\\&\equiv\tilde{g}_{\rm BBS}(\mathbf{K},\mathbf{k}';\omega)\delta\left[k'_0-\left[\frac{E_{p'_1}-E_{p'_2}}{2}\right]\right]\ .\end{aligned} \tag{A6}$$

In the above equation Λ_+ denotes the projection operator onto the positive-energy states. In particular,

$$\Lambda_+(\mathbf{p})=\sum_s|u(\mathbf{p},s)\rangle\langle\bar{u}(\mathbf{p},s)|\ , \tag{A7}$$

where

$$u(\mathbf{p},s)=\left[\frac{E_p+m}{2m}\right]^{1/2}\begin{bmatrix}1\\ \dfrac{\boldsymbol{\sigma}\cdot\mathbf{p}}{E_p+m}\end{bmatrix}\chi_s \tag{A8}$$

is the positive-energy Dirac spinor and k_0 is the timelike component of the four-vector k_μ.

Equation (A2a) in momentum space becomes (within the approximations described above)

$$\hat{T}(\mathbf{K},\mathbf{k}',\mathbf{k})=\hat{V}(\mathbf{K},\mathbf{k}',\mathbf{k})+\int d^3k''\hat{V}(\mathbf{K},\mathbf{k}',\mathbf{k}'')\tilde{g}_{\rm BBS}(\mathbf{K},\mathbf{k}'',\mathbf{k})\hat{T}(\mathbf{K},\mathbf{k}'',\mathbf{k})\ , \tag{A9}$$

where $\mathbf{k}'$, $\mathbf{k}''$, and $\mathbf{k}$ denote final, intermediate, and initial relative momenta, respectively, as defined by Eq. (2.2) and $\mathbf{p}_1,\mathbf{p}_2$ and ω have been expressed in terms of relative and total momenta.

Taking the matrix-element of the above equation with the positive-energy Dirac spinors $u(\mathbf{p},s)$ one obtains

$$\tilde{T}(\mathbf{K},\mathbf{k}',\mathbf{k})=\tilde{V}(\mathbf{K},\mathbf{k}',\mathbf{k})+\int d^3k''\tilde{V}(\mathbf{K},\mathbf{k}',\mathbf{k}'')g_{\rm BBS}(\mathbf{K},\mathbf{k}'',\mathbf{k})\tilde{T}(\mathbf{K},\mathbf{k}'',\mathbf{k})\ , \tag{A10}$$

where

$$\tilde{W}(\mathbf{K},\mathbf{k}',\mathbf{k})\equiv\langle\bar{u}(\mathbf{p}'_1,s'_1)\bar{u}(\mathbf{p}'_2,s'_2)|\,\hat{W}\,|u(\mathbf{p}_1,s_1)u(\mathbf{p}_2,s_2)\rangle \tag{A11}$$

for $\hat{W}$ either $\hat{V}$ or $\hat{T}$ and $g_{\rm BBS}(\mathbf{K},\mathbf{k}'',\mathbf{k})$ is equal to $\tilde{g}_{\rm BBS}(\mathbf{K},\mathbf{k}'',\mathbf{k})$ of Eq. (A9) without the projectors $\Lambda_+(\mathbf{p}_1)\Lambda_+(\mathbf{p}_2)$.

In the nucleon-nucleon (NN) c.m. frame ($\mathbf{K}=0$), Eq. (A10) becomes

$$\tilde{T}(\mathbf{k}',\mathbf{k})=\tilde{V}(\mathbf{k}',\mathbf{k})+\int d^3k''\left[\frac{m}{E_{k''}}\right]\tilde{V}(\mathbf{k}',\mathbf{k}'')\frac{1}{k^2/m-k''^2/m+i\eta}\tilde{T}(\mathbf{k}'',\mathbf{k})\ , \tag{A12}$$

where we have used the explicit form of $g_{\rm BBS}(\mathbf{K}=0,\mathbf{k}'',\mathbf{k})$ in addition to the fact that

$$\omega=4K_0^2-4K^2=4K_0^2=(E_{p_1}+E_{p_2})^2$$
$$=4E_k^2=4(k^2+m^2)$$

in the NN c.m. frame. For simplicity, we have also omitted the total momentum $\mathbf{K}=0$ as an argument of $\tilde{V}$ and $\tilde{T}$.

If we now multiply both sides of Eq. (A12) by the factor $\sqrt{m/E_{k'}}\sqrt{m/E_k}$ and define the quantities

$$V(\mathbf{k}',\mathbf{k})=\sqrt{m/E_{k'}}\tilde{V}(\mathbf{k}',\mathbf{k})\sqrt{m/E_k}\ ,$$
$$T(\mathbf{k}',\mathbf{k})=\sqrt{m/E_{k'}}\tilde{T}(\mathbf{k}',\mathbf{k})\sqrt{m/E_k}\ , \tag{A13}$$

we get

$$T(\mathbf{k}',\mathbf{k})=V(\mathbf{k}',\mathbf{k})+\int d^3k''V(\mathbf{k}',\mathbf{k}'')\frac{1}{k^2/m-k''^2/m+i\eta}\times T(\mathbf{k}'',\mathbf{k}) \tag{A14}$$

which is formally identical to the nonrelativistic Lippmann-Schwinger equation. The relationship between the NN differential cross section in the NN c.m. system and the scattering amplitude T as given by Eq. (A14) is

$$\frac{d\sigma}{d\Omega}=\left[\frac{m}{4\pi\hbar^2c^2}\right]^2|T(\mathbf{k}',\mathbf{k})|^2\ . \tag{A15}$$

The close similarity between the three-dimensional Blankenbecler-Sugar equation and the nonrelativistic Lippmann-Schwinger equation has motivated the use of the potential V, as given by Eq. (A13) and constructed from the relativistic meson-exchange theory, within the conventional nonrelativistic framework. However, as we have seen [Eqs. (A6) and (A10)], this similarity holds only in the NN c.m. frame. In other frames the Blankenbecler-Sugar equation is manifestly different (formally) from the Lippmann-Schwinger equation. Nevertheless, we consider the potential V given by Eq. (A13) as a nonrelativistic potential in the sense that we will use it in a nonrelativistic context such as in the Lippmann-Schwinger or Bethe-Goldstone equation. In the bound state problem the formal difference between the Blankenbecler-Sugar and Bethe-Goldstone equation has been shown to have little influence on the resulting interaction.[42]

Another notable point is related to the factors $\sqrt{m/E_p}$ in the definition of the interaction. The G-matrix or t-matrix interaction to be used in nonrelativistic calculations (and which has been represented by a sum of Yukawa terms in momentum space) is given by

$$G=\sqrt{m/E_{p_1'}}\sqrt{m/E_{p_2'}}\langle\bar{u}(\mathbf{p}_1')\bar{u}(\mathbf{p}_2')|\hat{G}|u(\mathbf{p}_1)u(\mathbf{p}_2)\rangle\sqrt{m/E_{p_1}}\sqrt{m/E_{p_2}}\ , \tag{A16}$$

where $\hat{G}$ denotes either $\hat{T}$ of Eq. (A9) or its Bethe-Goldstone analogue and $u(\mathbf{p})$ denotes the free nucleon spinor $u(\mathbf{p},s)$ *without* the two-component spin-wave function χ_s. Note that, apart from the factors $\sqrt{m/E_p}$, Eq. (A16) for the t matrix is identical to $\tilde{T}$ given by Eq. (A11) without the spin-wave functions χ_s.

In the Bethe-Goldstone equation, we use the OBEP which contains the factor $\sqrt{m/E_{k'}}\sqrt{m/E_k}$ as defined in Eq. (A13); therefore, the resulting G matrix also contains this factor so that the G-matrix interaction used in scattering calculations and given by the left-hand side of Eq. (A16) is related to that ($G^{\rm BG}$) obtained by solving the Bethe-Goldstone equation via

$$G=\sqrt{m/E_{p_1'}}\sqrt{m/E_{p_2'}}\sqrt{E_k'/m}\sqrt{m/E_{p_1}}\sqrt{m/E_{p_2}}\sqrt{E_k/m}\,G^{\rm BG}\ . \tag{A17}$$

The final point is related to the assumption involved in the use of the OBEP V when the Bethe-Goldstone equation is solved in practice. In the free NN problem the scattering equation is usually solved in the NN c.m. system [see Eqs. (A12)–(A14)] in a partial-wave helicity basis. The latter is simply related to the familiar $|JLS\rangle$ basis. Use of the helicity basis is extremely cumbersome in frames other than the NN c.m. frame as is required in nuclear matter calculations where one works in a frame in which the nuclear matter is at rest. Nevertheless, we use the partial-wave helicity matrix elements of the OBEP evaluated in the NN c.m. frame in subsequent calculations in the nuclear matter rest frame. This means that we are neglecting the c.m. momentum ($\mathbf{K}$) dependence of the OBEP which is questionable because, in contrast to bound state problems where the c.m. momentum is limited to $|\mathbf{K}|\leq k_F$, one has $|\mathbf{K}|>k_F$ for the unbound state cases. Here, however, we simply assume that the dependence of the OBEP on $\mathbf{K}$ is negligible.

[1]F. A. Brieva and J. R. Rook, Nucl. Phys. **A297**, 206 (1978); C. Mahaux, *ibid.* **A396**, 9c (1983); and N. Yamaguchi, S. Nagata and T. Matsuda, Proj. Theor. Phys. **70**, 459 (1983).

[2]H. V. von Geramb, in *The Interaction Between Medium Energy Nucleons in Nuclei*, edited by H. O. Meyer (AIP, New York, 1983), p. 44; L. Rikus, K. Nakana, and H. V. von Geramb, Nucl. Phys. **414**, 413 (1984); L. Rikus and H. V. von Geramb, Nucl. Phys. **A42**, 496 (1984).

[3]J. Kelly *et al.*, Phys. Rev. Lett. **45**, 2012 (1980); J. Kelly, in *The Interaction Between Medium Energy Nucleons in Nuclei,* edited by H. O. Meyer (AIP, New York, 1983), p. 153; J. Kelly, in *Relations Between Structure and Reactions in Nuclear Physics,* edited by D. H. Feng, M. Vallieres, and B. H. Wildenthal (World-Scientific, Singapore, 1987) p. 222.

[4]R. Machleidt, K. Holinde, and Ch. Elster, Phys. Rep. **149**, 1 (1987); R. Machleidt, private communication.

[5]M. Lacombe *et al.*, Phys. Rev. C **21**, 861 (1980).

[6]K. A. Brueckner and J. L. Gammel, Phys. Rev. **109**, 102 (1958).

[7]J. P. Jeukenne, A. Lejeune, and C. Mahaux, Phys. Rep. C **25**, 83 (1976).

[8]Z. Y. Ma and T. T. S. Kuo, Phys. Lett. **127B**, 137 (1983).

[9]M. I. Haftel and F. Tabakin, Nucl. Phys. **A158**, 1 (1970).

[10]M. L. Goldberger and K. M. Watson, *Collision Theory* (Wiley, New York, 1964); A. K. Kerman, H. McManus, and R. M. Thaler, Ann. Phys. **8**, 551 (1959).

[11]K. Nakayama, S. Krewald, J. Speth, and W. G. Love, Nucl. Phys. **A431**, 419 (1984).

[12]K. Nakayama, S. Krewald, and J. Speth, Nucl. Phys. **A451**, 243 (1986).

[13]K. Holinde, K. Erkelenz, and R. Alzetta, Nucl. Phys. **A198**, 598 (1972).

[14]K. Nakayama, S. Krewald, J. Speth, and W. G. Love, Phys. Rev. C **31**, 2307 (1985).

[15]W. G. Love and Amir Klein, J. Phys. Soc. Jpn. **55**, 78 (1985).

[16]W. G. Love and M. A. Franey, Phys. Rev. C **24**, 1073 (1981); M. A. Franey and W. G. Love, *ibid.* **31**, 488 (1985).

[17]M. H. Macfarlane and E. F. Redish, Phys. Rev. C **37**, 2245 (1988).

[18]W. G. Love and J. R. Comfort, Phys. Rev. C **29**, 2135 (1984); W. G. Love and Amir Klein, Proceedings of the LAMPF Workshop on Dirac Approaches to Nuclear Physics, Los Alomos, New Mexico, 1985, LAMPF Report No. LA-10438-C, 1985 (unpublished); D. A. Sparrow *et al.*, Phys. Rev. Lett. **54**, 2207 (1985).

[19]R. A. Arndt *et al.*, Phys. Rev. D **28**, 97 (1983); R. A. Arndt and L. D. Roper (unpublished).

[20]S.-O. Bäckman, G. E. Brown, and J. A. Niskanen, Phys. Rep. **124**, 1 (1985); G. E. Brown, J. Speth, and J. Wambach, Phys. Rev. Lett. **46**, 1057 (1981).

[21]E. Clementel and C. Villi, Nuovo Cimento **2**, 176 (1955).

[22]T. A. Carey *et al.*, Phys. Rev. Lett. **53**, 144 (1984); T. Carey, J. Phys. Soc. Jpn. Suppl. **55**, (1986), and references therein; H. Esbensen and G. F. Bertsch, Ann. Phys. **157**, 255 (1984); C. Glashausser *et al.*, (unpublished).

[23]W. G. Love, A. Klein and M. A. Franey, in *Antinucleon-and-Nucleon-Nucleus Interactions,* edited by G. E. Walker, C. D. Goodman, and C. Olmer (Plenum, New York, 1985), p. 1.

[24]W. D. Cornelius, J. M. Moss, and T. Yamaya, Phys. Rev. C **23**, 1364 (1981); S. J. Seestrom-Moris *et al.*, Phys. Rev. C **26**, 213 (1982); J. B. McClelland *et al.*, Phys. Rev. Lett. **52**, 98 (1984); J. M. Moss, in *Spin Excitations in Nuclei,* edited by F. Petrovich *et al.* (Plenum, New York, 1984), p. 355.

[25]F. Petrovich, H. Manus, V. A. Madsen, and J. Atkinson, Phys. Rev. Lett. **22**, 895 (1969); W. G. Love, Nucl. Phys. **A312**, 160 (1978).

[26]C. W. DeJager, H. de Vries, and C. De Vries, Atomic Data Nucl. Data Tables **14**, 479 (1974), and references therein.

[27]Alan Scott *et al.* (unpublished).

[28]W. G. Love, Amir Klein, M. A. Franey, and K. Nakayama, in *Medium Energy Nucleon and Antinucleon Scattering,* edited by H. V. von Geramb (Springer-Verlag, New York, 1985), p. 160.

[29]J. R. Comfort *et al.*, Phys. Rev. C **26**, 1800 (1982).

[30]S. Cohen and D. Kurath, Nucl. Phys. **73**, 1 (1965).

[31]M. Haji-Saeid *et al.*, Phys. Rev. C **25**, 3035 (1982).

[32]W. G. Love and M. A. Franey, J. Phys. (Paris) Colloq. **45**, Suppl. 3, C4-231 (1984).

[33]M. Kamimura. Nucl. Phys. **A351**, 456 (1981).

[34]T. Cheon, K. Takayanagi, and K. Yazaki, Nucl. Phys. **A437**, 301 (1984); **A445**, 227 (1985).

[35]B. D. Anderson *et al.*, Phys. Rev. C **31**, 1147 (1985); **34**, 422 (1986).

[36]W. G. Love, K. Nakayama, and M. A. Franey, Phys. Rev. Lett. **59**, 1401 (1987).

[37]F. Ajzenberg-Selove, Nucl. Phys. **A449**, 1 (1986).

[38]T. N. Taddeucci *et al.*, Phys. Rev. C **25**, 1094 (1981); J. Rapaport *et al.*, Phys. Rev. Lett. **54**, 2325 (1985); W. P. Alford *et al.*, Phys. Lett. B **179**, 20 (1986).

[39]R. A. Lindgren and F. Petrovich, in *Spin Excitations in Nuclei,* edited by F. Petrovich *et al.*, (Plenum, New York, 1984), p. 323; C. Olmer *et al.*, Phys. Rev. C **29**, 361 (1984); N. M. Hintz *et al.*, *ibid.* **30**, 1976 (1984).

[40]R. Schaeffer and J. Raynal (unpublished).

[41]J. Carr, J. Kelly, and F. Petrovich (unpublished).

[42]K. Nakayama, S. Drozdz, S. Krewald, and J. Speth, Nucl. Phys. **A470**, 573 (1987).

[43]The Bitnet address is WGLOVE@USCN.

[44]E. E. Salpeter and H. A. Bethe, Phys. Rev. **84**, 1232 (1951).

[45]R. Blankenbecler and R. Sugar, Phys. Rev. **142**, 1051 (1966); M. Partovi and E. Lomon, Phys. Rev. D **2**, 1999 (1970).

[46]R. Thompson, Phys. Rev. D **1**, 110 (1970).

[47]K. Erkelenz, Phys. Rep. C **13**, 191 (1974).

[48]J. D. Bjorken and S. D. Drell, *Relativistic Quantum Mechanics* (McGraw-Hill, New York, 1964).